



Jack of all trades: Versatile Catechol Crosslinking Mechanisms

Journal:	<i>Chemical Society Reviews</i>
Manuscript ID:	CS-REV-05-2014-000185.R2
Article Type:	Review Article
Date Submitted by the Author:	25-May-2014
Complete List of Authors:	Yang, Juan; Wageningen University, Cohen-Stuart, Martien; Wageningen University, Laboratory of Physical Chemistry and Colloid Science Kamperman, Marleen; Wageningen University, Physical Chemistry and Colloid Science

Jack of all trades: Versatile Catechol Crosslinking Mechanisms

Juan Yang, Martien A. Cohen Stuart and Marleen Kamperman*

Laboratory of Physical Chemistry and Colloid Science, Wageningen University, Dreijenplein 6,
6703HB Wageningen, the Netherlands

* Corresponding author: marleen.kamperman@wur.nl

Key words: catechol, crosslinking chemistry, Michael-type addition, Schiff base, polydopamine, metal coordination

Abstract

Catechols play an important role in many natural systems. They are known to readily interact with both organic (e.g., amino acids) and inorganic (e.g., metal ions, metal oxide) compounds, thereby providing a powerful system for protein curing. Catechol cross-linked protein networks, such as sclerotized cuticle and byssal threads of the mussel, have been shown to exhibit excellent mechanical properties. A lot of effort has been devoted to mimic the natural proteins using synthetic catechol-functionalized polymers. Despite the success in developing catechol-functionalized materials, the crosslinking chemistry of catechols is still a subject of debate. To develop materials with controlled and superior properties, a clear understanding of the crosslinking mechanism of catechols is of vital importance. This review describes the crosslinking pathways of catechol and derivatives in both natural and synthetic systems. We discuss existing pathways of catechol crosslinking and parameters that affect the catechol chemistry in detail. This overview will point towards a rational direction for further investigation of the complicated catechol chemistry.

1 Introduction

2 Curing of catechol-based materials by covalent crosslinking

2.1 Catechol oxidation

2.1.1 Enzymatic oxidation

2.1.1.1 Oxidation mechanism using tyrosinase

2.1.1.2 Influence of pH and ring substituents

2.1.2 Chemical oxidation of catechols

2.2 Secondary reaction of *o*-quinone with nucleophilic groups

2.2.1 The interaction of *o*-quinone with amines

2.2.1.1 Michael-type addition

2.2.1.2 Schiff base reaction

2.2.1.3 Strecker degradation

2.2.2 Reaction between catechols with thiols

2.2.3 Aryloxy radical coupling

2.3 Polydopamine formation mechanism and possible structures

3 Crosslinking mechanism of catechol-based system in the presence of transition metal ions

3.1 Fe³⁺-catechol coordination

3.2 Covalent crosslinking mediated by Fe³⁺

3.3 Interaction between catechol and other metal ions

4 Conclusions and outlook

1 Introduction

Catechols are prevalent in many natural systems; playing an essential role in living organisms such as mussels, sandcastle worms and squids,¹⁻⁴ and in food processing such as cocoa fermentation and tea preparation⁵⁻⁸. A famous example is the mussel that secretes water-resistant adhesive proteins containing significant amounts of the catechol-containing amino acid 3,4-dihydroxyphenylalanine (dopa).⁹ In 1981, Waite and Tanzer identified dopa as a key element for the enduring fixation of mussels to various types of surfaces under harsh marine conditions.⁹ Since then, a lot of research has been performed, trying to unveil the exact roles of catechols in mussel adhesion. Six mussel foot proteins (mfps) containing dopa have been identified.¹⁰ Though a complete understanding of the roles of catechol in mussel adhesion is still missing, significant progress has been made and many possible mechanisms have been proposed. Two aspects of the function of catechol in mfps are partly understood: adhesion and cohesion. For adhesion, mfps containing relatively high concentrations of dopa (e.g., 20 and 25 mol% dopa for mfp-3 and mfp-5, respectively¹¹) are present at the interface. The high concentration of dopa may enable strong interactions between catechol and organic or inorganic substrates, thereby ensuring water-resistant adhesion to various surfaces.^{12,13} Several modes of interaction between catechol and different surfaces have been described in excellent reviews.^{12,14} The cohesive properties of the mfps are related to the formation of load-bearing joints during the curing of the freshly secreted mfps, which are secreted as viscous fluids. The curing process of mfps relies on the versatile chemistry of catechols.¹⁵⁻¹⁷ Chemists have been inspired by the unique properties of the glues secreted by marine organisms, and the incorporation of catechol functionality into synthetic materials and subsequent crosslinking has aroused much interest.¹⁸⁻²⁰ Some synthetic materials have shown excellent properties. For instance, del Campo et al. developed nitrodopamine-ended four-arm

poly(ethyleneglycol) (PEG-ND₄). By mixing the material with Fe³⁺ (molar ratio Fe³⁺/PEG-ND₄ = 3: 1), a gel was formed through the complexation between Fe³⁺ and catechols in PEG-ND₄. The crosslinked material showed self-healing behavior and could be easily degraded by exposure to UV light. These two properties make this dopa-inspired material promising for cell biology and medical applications.¹⁹ Another well-known example inspired by mussels is polydopamine. Lee et al. reported a method to form multifunctional polymer coatings through simple dip-coating of objects in a Tris buffer (pH = 8.5) of dopamine. Using this method, a thin but robust film having a thickness ranging from a few nm to > 100 nm was deposited on virtually any material surface.²⁰ The versatility of this method with respect to the material of the substrate has opened up new possibilities for extraordinary applications, such as surface coating, biotechnology and biomedicine.²¹⁻²³ A comprehensive summary of all the catechol-based biomimetic functional materials has been given elsewhere.^{24,25}

Despite the success in fabricating catechol-based functional materials, the versatile chemistry of catechols, including the structure of polydopamine, is still a subject of debate. To advance the subject, and to provide a basis for the creation of superior materials, a clear understanding of the catechol reaction mechanisms is mandatory. An overview of the existing pathways of catechol crosslinking in natural protein systems and in synthetic mimics will, on one hand, help in gaining a full picture of the current status in this field; and on the other hand, point towards a rational direction for further investigation of the complicated catechol chemistry. Fig. 1 presents a brief scheme of the crosslinking chemistry of catechols. Catechols are easily oxidized to form reactive *o*-quinones²⁶, which then can undergo secondary reactions to form covalent crosslinks.^{27,28} In addition, catechols can interact with transition metals by forming strong coordination bonds to give catechol-metal complexes.¹²

The details of the various crosslinking mechanisms are the topic of this review. As similar remarkable crosslinking chemistries of catechol have been observed in other living organisms,

such as sandcastle worms,² and squid beaks,¹ studies based on these organisms will be discussed, too. Moreover, catechols, or more generally, phenols are also prevalent in natural food products, such as tea, wine, tobacco.⁵⁻⁸ The oxidized phenols can also react with free amino acids, peptides, proteins or quinonic compounds, resulting in a phenomenon called “enzymatic browning”. The browning of the food adversely affects the quality of food, e.g., color, aroma and flavor. A detailed overview of the browning of natural products has been reviewed in other work.²⁹ The chemistry of this effect, i.e., possible reactions between quinone and amino acids will be discussed in this review.

This review will be structured according to the possible crosslinking mechanisms of catechol that have been proposed so far, regardless whether the described system is natural or synthetic. Section 2 will focus on the catecholic covalent crosslinking mechanism in the absence of transition metals (e.g. Fe^{3+}), unless otherwise mentioned. This section will be divided into three sub-sections. In section 2.1, we will discuss the one or two-electron enzymatic or non-enzymatic oxidation of catechols to form *o*-quinone. The effect of pH, redox potential, and substitution on the catecholic benzene ring, etc., on the oxidation will be reviewed. In section 2.2, we will present the current knowledge on the subsequent secondary reactions of *o*-quinone with nucleophilic groups. This section comprises three sub-sections: i) Section 2.2.1 will focus on the reaction of *o*-quinone with amines; ii) Section 2.2.2 will focus on the reaction of thiol groups; and iii) Section 2.2.3 will focus on the reverse dismutation of *o*-quinone with catechols to form aryl radicals, which can further couple to form crosslinks. The proposed formation mechanism of polydopamine and its possible structures will be reviewed in section 2.3. In section 3, the affinity of catechol to transition metals, mainly focusing on Fe^{3+} , will be reviewed. Finally, section 4 will conclude with an overview of all possible reactions identified so far.

2 Curing of catechol-based materials by covalent crosslinking

2.1 Catechol oxidation

Catechols have been known for more than 70 years to be susceptible to oxidation upon exposure to air.³⁰ This spontaneous oxidation of catechol in the presence of oxygen is referred to as “auto-oxidation”. In the auto-oxidation step, catechols undergo sequential abstraction of two electrons with the concomitant loss of two hydrogen atoms (Fig. 2). The first step is the one-electron oxidation of catechol to the *o*-semiquinone radical, during which O_2^- is formed. The formed O_2^- then reacts with catechol to form an *o*-semiquinone radical and H_2O_2 . The formation of *o*-semiquinone has been identified^{31,32} and detected by electron paramagnetic resonance (ESR) using continuous flow methods.³³ The formed *o*-semiquinone radicals are transient, and they decay rapidly through disproportionation to form *o*-quinone and catechol. The redox reaction between catechol and oxygen under biological conditions (i.e. air-saturated solution, around pH 7 and less than 10^{-2} M catecholic material) is thermodynamically unfavorable. For step 1 of the auto-oxidation of catechol, at pH 7, the redox potential of the pair catechol/*o*-semiquinone is 530 mV,³⁴ while the redox potential of O_2/O_2^- is -155 mV.^{35,36} Therefore, the equilibrium in step 1 is biased to the left, i.e., the oxidation of catechol is all but complete.

2.1.1 Enzymatic oxidation

In natural systems, the obstacle of catechol auto-oxidation, i.e., the high activation energy barrier is overcome by the presence of enzymes (e.g. tyrosinase, horseradish peroxidase/ H_2O_2) or metal ions (e.g. Fe^{3+}). The mechanism of the reaction catalyzed by tyrosinase is a two-electron oxidation process, while for horseradish peroxidase/ H_2O_2 it is a one-electron oxidation process. The catechol oxidation by transition metal ions will be discussed in section 3.

Tyrosinase is widely present in living organisms.³⁷ Tyrosinase belongs to a larger class of copper-containing proteins; these proteins are able to bind oxygen (Fig. 3). A common feature

is the presence of a binuclear copper site coordinated by six histidines.³⁸⁻⁴⁰

2.1.1.1 Oxidation mechanism using tyrosinase

A lot of research has been performed to study the effect of tyrosinase on phenol (including catechol) oxidation. The detailed function of tyrosinase on phenol oxidation has been reviewed by Riley et al.⁴¹ Here, we briefly discuss the mechanism of tyrosinase-catalyzed oxidation of catechol based on the study of the electronic structures of active sites of tyrosinase.⁴² The electronic structures of the copper site were studied by spectroscopic methods (e.g. Raman, electron paramagnetic resonance) and quantum mechanics calculations. Catechol oxidation catalyzed by tyrosinase involves two steps: (i) the activation of tyrosinase (Fig. 4) and (ii) the catecholic oxidation cycle by the activated tyrosinase (Fig. 5). The initial tyrosinase is in its inactive *met*-tyrosinase form, in which the binuclear copper site is in the wrong oxidation state to bind oxygen.⁴² In the presence of catechols, *met*-tyrosinase is converted to *deoxy*-tyrosinase. Meanwhile, the catechols are oxidized by the two-electron transfer process, in which an *o*-semiquinone radical is formed in a secondary reaction between *o*-quinone and catechol, as described in Fig. 5. The *deoxy*-tyrosinase readily binds oxygen to give *oxy*-tyrosinase, which can oxidize catechol to form *o*-semiquinone and quinone.

As shown in Fig. 6, by oxidizing catechol to *o*-quinone, *oxy*-tyrosinase is reduced to *met*-tyrosinase, which cannot bind oxygen to regenerate *oxy*-tyrosinase. Only in the presence of a second catechol the *met*-tyrosinase is activated again. The inactivation of tyrosinase during catechol oxidation has also been proposed by Dawson and co-workers, who studied the catechol oxidation in a buffered tyrosinase-catechol system using polarimetry.^{43,44}

The extent of oxygen consumption during the enzymatic oxidation of catechol has been studied and appears controversial. Several investigations reported that for complete oxidation of catechols, two oxygen atoms are needed per catechol molecule.⁴⁵⁻⁴⁷ Wright and Mason reported, however, that the consumption of oxygen depends on the enzyme and catechol

concentration.⁴⁸ When the enzyme concentration was less than 3.3 catecholase units per ml of reaction volume, the oxygen atom consumption increased to 2.5 oxygen atom per catechol molecule. A further increase in enzyme concentration did not lead to an increase in oxygen consumption. Wright and Mason also showed that a higher concentration of catechol results in a lower oxygen consumption.

2.1.1.2 Influence of pH and ring substituents

The oxidation kinetics of catechols by tyrosinase can be affected by several parameters, such as pH and the nature of ring substituents of catechol. The effect of pH on the catechol oxidation can be described in relation to reduction potentials. As mentioned before, the one-electron reduction potential of catechol/semiquinone is 530 mV at pH 7.³⁴ At pH 11, one of the catecholic hydroxyl groups is deprotonated, leading to a lower one-electron reduction potential of 98 mV.³⁴ Therefore, deprotonation shifts the reaction equilibrium in Fig. 2 towards the right side. This effect of alkaline conditions on catechol oxidation has been extensively reported.⁴⁹⁻⁵¹ Wright and Mason studied the catechol oxidation in presence of tyrosinase at pH 3, 4, 5 and 7. It was found that when the pH was increased, the initial rate of oxidation was increased.⁴⁸

The nature of ring substituents of catechol also affects the oxidation kinetics through its steric, hydrophobic and electronic properties. According to Riley, the oxidation of catechol by tyrosinase can be described as depicted in Fig. 7, in which k_1 is the oxidation rate and k_2 is the rate of inactivation of tyrosinase.⁴³

The oxidase activity ($\log k_1$) can be approximated using the following empirical relationship (1), in which π describes the hydrophobicity of the substituent and L describes its length, i.e., whether the substituent is long or short.

$$\log k_1 = 0.364(\pm 0.097)\pi - 0.297(\pm 0.077)L + 2.369 \quad (1)$$

By investigating the oxidation kinetics of catechols with different substituents on the 4-position, Ramsden and Riley demonstrated that shorter substituents (smaller L) or more hydrophobicity (larger π) gave faster oxidation rates; and larger substituents (larger L) or more hydrophilic substituents (smaller π) resulted in slower oxidation.⁴³

The electronic properties of the substituents also affect the oxidation rates. For substituents that are more electron-withdrawing (such as NO_2 , CN , CF_3), catechols become difficult to oxidize.^{43,52} In contrast, substituents that are more electron-donating (such as $-\text{OMe}$, $-\text{Me}$) stabilize the radicals, resulting in the opposite effect.⁵³ These effects of the substituents may also be applicable for other oxidants with different oxidation mechanisms. However, more in-depth studies are needed to clarify this. In addition, it should be noted that these effects were found for 4-substituted catechols. Whether these effects are applicable to substituents at other positions is still an open question.

2.1.2 Chemical oxidation of catechols

Catechols are also readily oxidized in the presence of chemical oxidants. The most commonly used oxidants are sodium periodate^{15,54} and silver oxide⁵⁵. The periodate-mediated oxidation proceeds via a two-electron oxidation, and that for silver oxide proceeds via a one-electron oxidation reaction.^{56,57} A clear understanding of the reaction mechanism of periodate-oxidation of catechol is lacking. Nevertheless, Kaiser et al. have proposed three reaction pathways, based on investigations on the oxidation of catechol by sodium periodate with a stopped flow apparatus at different pH, ranging from 0 to 10.⁵⁸⁻⁶⁰ They detected an intermediate during the oxidation without identifying the nature of the product. It was proposed that the intermediate was a cyclic diester of periodic acid. Two possible structures were suggested, as indicated in Fig. 8 (a) and (b).

The intermediates were proposed to be able to decompose to *o*-quinone via three pathways (Fig. 8).

To summarize, catechols in both synthetic mimics and natural systems are susceptible to aerobic oxidation. The oxidation process is influenced by pH and aromatic ring substituents on catechols. In general, a higher pH leads to a higher oxidation rate. Catechols with aromatic ring substituents that have electron-withdrawing properties (NO_2 , CN , CF_3) are more difficult to oxidize; while those with substituents that have electron-donating properties ($-\text{OMe}$, $-\text{Me}$) are easier to oxidize. For enzymatic oxidation of catechols, the mechanism has been well studied. The inactive tyrosinase is first activated to its reactive state *deoxy*-tyrosinase, which then catalyzes catechol to undergo a two-electron oxidation process. For the oxidation of catechols in the presence of chemical oxidants, such as sodium periodate, the mechanism is not well understood. It is proposed that catechols and sodium periodate form a cyclic diester of periodic acid as an intermediate, which ultimately forms *o*-quinone.

2.2 Secondary reaction of *o*-quinone with nucleophilic groups

The *o*-quinone groups are unstable intermediates and highly reactive electrophilic molecules that can further undergo several secondary reactions to form reddish brown or black pigments. These secondary reactions comprise: a) reactions with amine groups, b) reactions with thiol groups; c) aryloxy radical coupling. In the following sections, we will elaborate on the three reaction ways one by one.

2.2.1 The interaction of *o*-quinone with amines

O-quinones can react with amines through three pathways: i) Michael-type addition; ii) Schiff base reaction and iii) Strecker degradation. In this review, the first two will be discussed in detail, and Strecker degradation will be discussed briefly in section 2.2.1.3. The factor that mainly determines which of these three reaction types will predominate is the type of amine.⁶¹ For example, Manthey et al. identified the oxidation products of catechol in the presence of two aliphatic (aniline and *p*-anisidine) and aromatic amines (2-phenylethylamine

and butylamine) using ^1H and ^{13}C NMR. They found that aromatic amines favor Michael-type addition (i.e., 4,5-disubstituted *o*-quinone adducts), and aliphatic amines favor Schiff base reaction (i.e., 2,4,5-trisubstituted or 2,4-disubstituted *o*-quinone adducts).⁶¹

2.2.1.1 Michael-type addition

Quinones undergo a nucleophilic attack by amines to form quinone-amine adducts. The complete reaction mechanism between *o*-quinone with primary amines has not been experimentally verified. However, it has been proposed that the mechanism between *o*-quinone and amine resemble that of *p*-quinone and amine.⁶² Therefore, in the following, we first show the reaction mechanism of *p*-quinone and amine, as indicated in Fig. 9.

The reaction is initiated by the addition of an amine to a carbon-carbon double bond, forming an intermediate (1). The intermediate is then isomerized to form aminohydroquinone (2), which is subsequently oxidized to form monoaminoquinone (3). The monoaminoquinone (3) reacts further with amine to produce diaminoquinone (5) via an intermediate (4).

Despite of the unclear mechanism, in natural living organisms and food processing, the formation of *o*-quinone-amino adducts have been identified. In many of these natural systems it involves a reaction between dopa and histidine. For instance, Waite et al. found dopa and several crosslink derivatives from the beak cutouts of squid *Dosidicus gigas*. They isolated protein fragments by phenylboronate chromatography followed by reverse-phase HPLC, and the fragments were measured by UV-Vis spectroscopy, ^1H NMR, electrospray ionization mass spectrometry, and tandem mass spectrometry. They identified that the hydrolyzed compounds obtained from the insoluble black pigments from squid beaks are multimers (dimer, trimer and tetramer) of catechol-histidine adducts.^{1,63} The structures of the multimers are shown in Fig. 10. The imidazole nitrogens either attach to the 2- or the 6-position (or both) on the aromatic ring of catechol in these adducts.

In addition, Turecek et al. characterized the catechol-amino acid adducts in acid hydrolysates

of sclerotized cuticles by mass spectroscopy and HPLC.⁶⁴ They identified the presence of C-N bonds, which had been formed between the nucleophilic imidazole N of histidine in cuticular protein and both the ring and side chain C of three sclerotization precursors, i.e. N-acetyldopamine, N-beta-alanyldopamine and 3,4-dihydroxyphenylethanol. The authors proposed a pathway for protein crosslinking by C-N bond formation during sclerotization, as shown in Fig. 11.⁶⁴ The substitution pattern (4-substituted) is different from the observations in Fig. 9. Up till now, it is not clarified at which position on the aromatic ring of *o*-quinone the amine is most likely to attach.

The presence of dopa-histidine crosslinks has also been reported in other work.⁶⁵⁻⁶⁷ The proposed structure of the crosslink structure is shown in Fig. 12.

In tobacco processing, the formation of *o*-quinone-amine adducts has also been identified. During the drying process of tobacco, *o*-quinone reacts with nor nicotine, resulting in a red color absorbing at 570 nm.^{68,69} A model reaction of nor nicotine with *o*-quinone is indicated in Fig. 13.²⁹ Products from both Michael addition and Schiff base reactions (which will be discussed in the next section) were formed.

Similar amino-catechol adducts from Michael addition were studied by Rafiee and co-workers. They employed cyclic voltammetry and controlled potential-coulometry to study the electrochemical oxidation of catechol (1) in the presence of sulfanilic acid (2) resulting in the formation of an amino-*o*-quinone derivative (3a) (Fig. 14).⁷⁰

Messersmith et al. identified quinone-amine adducts indirectly using atomic force microscopy measurements on the interaction of a single *N*-Boc-protected dopa residue in contact with an amine-containing Si surface.⁷¹ They found that the pull-off force is initially 2.2 nN at pH 9.7, after which, an additional contact/pull-off measurement showed no adhesion force. This result indicated that the formation of a covalent, irreversible dopa-N bond is possibly formed via Michael addition. Similar reactions between dopa and amines may also occur in mussel-

secreted proteins; however, no direct evidence of this exists up till now.

Parameters influencing Michael-type addition

Three parameters that affect the Michael addition of catechol and amine groups are pH, the type of catechol groups and the basicity of the nucleophile amines. For instance, Truscott et al. investigated the oxidation of catechol by tyrosinase in the presence of aniline at pH 7 and 11.7, respectively.⁶¹ By analyzing the aromatic and olefinic resonance in the ¹H and ¹³C NMR spectrum of the final products, they found that at pH 7, the majority of the products is 4,5-diarylamino-1,2-dihydrobenzene formed by Michael addition (Fig. 15 (a)) with small amounts (4%) of a compound formed by Schiff base reaction (Fig. 15 (d)) (as will be discussed in the next section). In comparison, at pH 11.7, only tautomers of 4,5-diarylamino-1,2-dihydrobenzene (Fig. 15 (a), (b) and (c)) were formed. pH also affects the reaction rate of Michael addition through the protonation state of the amines. For instance, Shirmohammadi et al. studied the reaction of electrochemically generated *o*-quinones and nucleophilic *N*-methylaniline by cyclic voltammetry.⁷² They found that the rate constant for Michael addition increases with increasing pH, up to pH 6. This trend is related to the deprotonation of the amine group. By increasing the pH to a value higher than 6, the rate constant slightly decreases. This decrease may be explained by the fact that the conversion of *o*-quinone to catechol needs proton exchange. An increase in reaction rate of *o*-quinone with amine groups with increasing pH was also reported for catechol oxidation in the presence of sulfanilic acid: At pH 3 the rate constant is 0.35 M⁻¹s⁻¹, while at pH 6.5, the calculated rate constant is 0.45 M⁻¹s⁻¹. At low pH, sulfanilic acid is protonated, yielding deactivated amine groups towards the Michael addition reaction with *o*-benzoquinone.⁷⁰ Therefore, the reaction rate is decreased. Similar observations have also been reported for the reaction between 3-substituted catechols with dibenzylamine.⁷³

The second parameter that affects Michael addition is the type of catechols. Shirmohammadi et al. studied the effect of catechol type on the kinetics of catechol oxidation in the presence of N-methylaniline.⁷² The reaction mechanism is shown in Fig. 16. They reported that the reactivity of catechol is higher than that of 4-methylcatechol. The lower reactivity of 4-methylcatechol is related to the steric effect of the methyl group. The occupation of methyl group reduces the probability of reaction by a factor of two. This reduced reactivity is also reflected in the difference in half-wave potential ($\Delta E_{1/2}$) of reactants (catechol/ 4-methylcatechol) and products (diphenylamine). $\Delta E_{1/2}$ for the catechol and 4-methylcatechol are 210 mV and 95 mV, respectively. By simulation, they also reported that the rate constants for the catechol and 4-methylcatechol are 1.23 and 0.42 $\text{M}^{-1}\text{s}^{-1}$, respectively. Besides the steric effect, the substitution group on the catechol ring also plays a role via its electronic properties. For substitution groups that are electronic-donating, they lead to a lower homogeneous rate constant in the Michael addition. For instance, the homogeneous rate constant in the case of catechol is 0.068 $\text{M}^{-1}\text{s}^{-1}$, while for 3-methylcatechol and 3-methoxycatechol these are 0.045 and 0.023 $\text{M}^{-1}\text{s}^{-1}$, respectively.⁷³

The Michael addition is also affected by the basicity of the nucleophilic amines. Kazemi and coworkers reported the oxidation of catechol in the presence of three secondary amines morpholine, dimethylamine and diethylamine.⁷³ The basicity trend of the three amines is decreasing in the order of diethylamine (basicity constant $k=1.05 \times 10^{-3}$), dimethylamine ($k=4.79 \times 10^{-4}$) and morpholine ($k=2.14 \times 10^{-6}$). At a fixed pH, the concentration of free amines that are active for Michael addition showed an increasing trend in the series of diethylamine, dimethylamine and morpholine. A higher concentration of nucleophile causes a higher reaction rate. Therefore, morpholine showed the highest reaction rate. In the presence of aromatic amines, when the pKa of aromatic amine is low (pKa \sim 5.0), the quinone-aromatic amine adducts even formed at acidic pH.^{74,75}

2.2.1.2 Schiff base reaction

O-quinone can also react with amines by Schiff base reaction. The reaction mechanism is unclear. However, the quinone-imines from Schiff base reaction have been detected using ^1H NMR. Horak and co-workers characterized the product (Fig 17 (3)) from the reaction between cyclohexylamine (Fig. 17 (2)) with 3,4-di-*tert*-butyl-1,2-benzoquinone (Fig. 17 (1)) using ^1H NMR.⁷⁶

The structures of the amine-catechol adducts have also been confirmed by characterization with FTIR. Feng et al. reported the reaction of poly(dopamine) with polyetherimide (PEI), and detected an absorption at 1623 cm^{-1} by FTIR. This absorption was attributed to the C=N stretch, which originates from a Schiff base formation.⁷⁷ The Schiff base reaction has also been identified for the reaction between lysine or polylysine with *o*-quinone.^{78,79} Burzio and Waite reported the coupling of a model catechol-containing decapeptide compound with the amino acid lysine or glycine.¹⁵ They analyzed the material by MALDI-TOF mass spectrometry, and found that the molar mass decreased by 18 after adding the amino acid to the oxidized decapeptide. This mass loss corresponds to a loss of one water molecule, which should be due to the Schiff base reaction between amine and *o*-quinone. Faure et al. have also indirectly observed the Schiff base product.⁸⁰ They reported that a nanogel formed from the reaction between a homopolymer of methacrylamide bearing 3,4-dihydroxy-L-phenylalanine (P(mdopa)) and poly(allylamine) at pH 10. They performed solid state ^{13}C NMR and found that the peak at a chemical shift of 160 ppm increased. They assigned this peak to the imine bond formed by the Schiff base reaction between oxidized *o*-quinone in P(mdopa) and the amines in poly(allylamine). When the oxidized *o*-quinones were occupied by metal ions, e.g. Ag^+ , the product showed increased peak intensity at a chemical shift of 140 ppm in solid state ^{13}C NMR, indicating the formation of an amine-catechol adduct formed by Michael

addition.⁸⁰

Parameters influencing Schiff base reaction

The Schiff base reaction is strongly affected by pH. As proposed by Manthey et al., the reaction between catechol and 2-phenylethylamine at neutral pH first forms a phenylethyl product (Fig. 18a) as the intermediate, which further transforms to imine-quinone adduct through Schiff base reaction (Fig. 18a).⁷⁹ At higher pH (11.7), as shown in Fig. 18b, the product is catalyzed to give an intermediate, which undergoes further Schiff base formation at the carbonyl of the vinylogous amide moiety rather than that of the less reactive vinylogous carboxylate anion.⁷⁹

Another parameter that strongly affects Schiff base reaction is the chain length of the compound containing the primary aliphatic amine. A longer chain length leads to a decrease in the basicity of the α -NH₂, which enables the formation of catechol-NH₂ at a lower pH. As reported by Sealy, the ease of forming catechol-amine adducts is GlyGlyGly > GlyGly > Gly.⁷⁴

2.2.1.3 Strecker degradation

O-quinone can also react with amines by Strecker degradation.²⁹ This reaction is an oxidative degradation at high temperature of α -amino acids by *o*-quinone (Fig. 19). During the reaction, critical intermediates, i.e. related aldehydes (Strecker aldehydes) and 2-aminocarbonyl compounds, are produced. Such compounds contribute to aromas in processed food. Though the reaction is important, it is beyond the scope of our review, since our focus is on the crosslinking reactions of catechols in living organisms and natural products, without involving the reaction under heating conditions. Yaylayan et al. has written an excellent review about this research field.⁸¹

To summarize, the reactive *o*-quinones react with nucleophilic amines, as indicated in Fig. 20, through three reaction pathways, i) Michael type addition, ii) Schiff base reaction and iii) Strecker degradation. In a Michael type addition an amine is attached to the catechol ring at the 4- or 5- position, and in a Schiff base reaction the amine attacks the 2- position at the catechol ring and an imine is created.

The reaction pathway between *o*-quinone and amine depends on the type of amine. Generally, aromatic amines favor Michael-type addition, whereas aliphatic amines favor Schiff base reaction. The quinone-amine adducts formed from these three mechanisms have been detected in both natural and synthetic mimics systems, such as cuticle sclerotization and natural food products. Three parameters can affect Michael type addition, i.e., pH, type of catechol groups and the basicity of nucleophile amines. In general, an increase in pH results in a higher reaction rate. Catechols with a substitute on its ring such as 4-methylcatechol reduce the reactivity when compared to catechols, mostly due to the steric effect of the methyl group. In addition, substituents that are electron donating also lead to a lower reaction rate. A third factor is the basicity of the nucleophilic amines. Generally, a more basic amine resulted in a higher reaction rate.

Schiff base reactions are affected by the pH and the chain length of the compound containing the primary amine. The pH for the formation of catechol-amine adducts can be tuned by the chain length of the primary aliphatic amine. A longer chain length leads to a decrease in the basicity of the primary amine, which allows the reaction to proceed at lower pH.

2.2.2 Reaction between catechols with thiols

The electrophilic *o*-quinone is highly reactive, and can react through Michael-type addition with nucleophilic thiol groups to form catechol-thiol adducts. The conjugation of the nucleophilic thiols to *o*-quinones was proposed to proceed as shown in Fig. 21.⁸² The catechol

and its derivatives are readily oxidized to form *o*-quinone. The quinones spontaneously undergo an attack by the nucleophilic thiol group at the 2-position of the ring, which leads to the regeneration of a catechol. The 2-substituted catechol moiety can be re-oxidized to form quinones. Thereafter, the resultant 2-substituted *o*-quinones undergo a second nucleophilic attack at the 5-position of the ring.

The presence of catechol-thiol adducts have been detected in many different systems.^{83,84} For instance, Waite and co-workers analyzed the components in cured glues secreted by the polychaete *Phragmatopoma californica*.² They found that the proteins contained 5-*S*-cysteinyl-dopa crosslinks that had been formed from dopa and cysteine during the setting process. The 5-*S*-cysteinyl-dopa has a molecular weight of 316.1 Da and the crosslink density was estimated to be one per 100 amino acids.² The same adduct has also been detected in the plaque footprints of California mussels *Mytilus californianus*. The crosslinked proteins could be isolated by acid hydrolysis due to the stability of catechol-thiol adducts in acid.^{2,15,85} The obtained compounds were characterized by UV-Vis spectrophotometry, electrospray ionization mass spectrometry and tandem mass spectrometry. In another type of mussel: the green shell mussel *perna canaliculus*, both 5-*S*-Cysteinyl-dopa and 2-*S*-Cysteinyl-dopa crosslinks were detected. 5-*S*-cysteinyl-dopa crosslinks were 10 times more abundant than 2-*S*-Cysteinyl-dopa, reaching more than 1 mol% in the threads. These two crosslinks could also be formed in vitro by incubating the protein (*perna canaliculus* foot protein pcfp-1) solution with tyrosinase at pH 7.5.² Mfp-6 is known to have high concentrations of cysteine (more than 11 mol%).^{3,86} The cysteine has a low pKa, which enables the formation of thiolate at pH 5.5 inside the mussel.⁸⁷ Since thiolates are more reductive than thiols, in mussel foot proteins, the thiolates are the operative antioxidant group.⁸⁸ The mechanism of dopaquinone reduction to catechol by thiolate is proposed to consist of two steps: i) nucleophilic attack of quinone by the first thiolate anion to form *S*-cysteinyl-dopa adducts; ii) the thioether adducts are attacked

by a second thiolate anion to form disulfide and dopa, as depicted in Fig. 22.³

Thiol-catechol adducts have also been identified in synthetic polymers. Yoo and co-workers prepared electrospun nanofibrous meshes from catechol-conjugated 8-arm poly(ethylene glycol) (8cPEGa) and thiolated poly(lactic-co-glycolic acid) (PLGA-SH). They identified the conjugation of thiol and catechol by comparing the Raman spectra differences between nanofibers before (NF) and after crosslinking (XNF) using sodium periodate solutions.⁸⁹ They identified peaks at 640-820 cm^{-1} and 2180-2290 cm^{-1} , which were ascribed to C-S or C-S-C and sulfur-hydrogen bonds, respectively. The peak intensity of C-S or C-S-C in XNF increased 40-fold compared to NF, while the peak intensity of sulfur-hydrogen bond signals decreased significantly. These observations indicated the conjugation of the sulfur atom of PLGA-SH to the carbon atom of 8cPEGa.⁸⁹ Messersmith et al. designed a bio-inspired composite hydrogel with excellent tissue-adhesion properties using the thiol-catechol reaction. The composite was prepared by mixing hyaluronic acid conjugated with dopamine (HA-DA) with a thiol end-capped Pluronic F127 (Plu-SH) in PBS buffer at pH 7.4. By using UV-Vis spectroscopy, oxidation of catechol in HA-DA resulted in quinones (absorbance peak at 375 nm), which subsequently reacted with Plu-SH via thiol-catechol linkage at pH 7.4 (absorbance at 293 nm and 615 nm).⁹⁰

Parameters influencing reaction between catechol and thiol

The addition efficiency of catechol to thiols depends on the oxidation rate of the catechols and on the nucleophilic strength of the thiols. In general, a higher oxidation rate of the catechols leads to a more efficient thiol-catechol conjugation. As reported by Darriet and co-workers, the type of catechol derivative affects the efficiency of catechol-thiol conjugation.⁹¹ By analyzing the addition products upon reaction of 3-sulfanyhexan-1-ol (3SH) with *o*-quinones derived from (+)-catechin, (-)-epicatechin and caftaric acid, it was found that the production

of adducts decreases in the order of catechin, epicatechin and caftaric acid. Another parameter that affects the addition efficiency is the nucleophilic strength of the thiols, which was modulated by the steric hindrance of the thiol groups. Primary thiols are more reactive than tertiary thiols.⁹² Nikolantonaki et al. reported the reactions between the thiols 3-sulfanyhexan-1-ol (3SH), 2-furanmethanethiol (2FMT) and 4-methyl-4-sulfanylpentan-2-one (4MSP) and the catechol derivatives (+)-catechin and (-)-epicatechin. They demonstrated that 4MSP was relatively less reactive towards *o*-quinones than 2FMT and 3SH. 2FMT, is a primary thiol and is expected to have the least sterically hindered sulfhydryl group of the three thiols. Therefore, 2FMT showed the highest reactivity with the quinones. In contrast, 3SH and 4MSP are secondary and tertiary thiols, respectively. The stronger steric hindrance resulted in lower reactivity.⁹³

To summarize, *o*-quinone undergoes a nucleophilic attack by thiols at the 2- and 5- position of the aromatic catechol ring, and thiol-catechol adducts are formed (Fig. 23). The addition efficiency of the reaction is increased by a higher oxidation rate of catechols. Moreover, primary thiols with less steric hindrance exhibit higher reactivity than secondary and tertiary thiols.

2.2.3 Aryloxy radical coupling

The *o*-quinone groups can also go through reverse dismutation to an unoxidized catechol, yielding two highly reactive semi-quinone radicals.^{15,37} The formed radicals can couple to form di-dopa crosslinks (Fig. 24).

Haemers and co-workers studied the oxidation and aggregation of mfp-1 under different conditions by using photo correlation spectroscopy and proposed a kinetic model for the crosslinking pathway.⁹⁴ The crosslinking kinetics are related to the rate of dopa oxidation and the rate of *o*-quinone dismutation to form semiquinone radicals. They studied the crosslinking

and aggregation of mfp-1 with and without the presence of a strong oxidizing reagent (iodate). In the presence of iodate, the dismutation of *o*-quinone with catechols is the rate-determining step, but the oxidation of catechol to *o*-quinone is very fast. Crosslinking stops when all dopa has been oxidized to *o*-quinone, resulting in limited crosslinking. Therefore, addition of an oxidizing reagent limits semiquinone radical formation, resulting in few crosslinks and small aggregates of mfp-1.

In the absence of a strong oxidizing reagent at high pH, Haemers and co-workers observed small particles at the beginning and large aggregates at the end of the reaction.⁹⁴ This observation indicates that the oxidation of catechol is the rate-determining step. This limitation causes dopa to remain available for the dismutation of *o*-quinone to form semiquinone radicals, so as to form more crosslinks and large aggregates. Increasing the pH in the absence of a strong oxidizing agent leads to faster catechol oxidation. In this way, more *o*-quinone can react with the remaining dopa to form more semiquinone radicals that can crosslinks. Therefore, a high pH yields a mfp-1 sample with more aggregates.

The presence of di-dopa crosslinks has also been identified in other natural systems.¹⁵ For instance, Waite et al. has identified the 5, 5'-di-dihydroxyphenylalanine crosslinks in the protein of *Mytilus edulis* by NMR spectroscopy studies.³⁷ In a different study the reactivity of peptidyl-dopa in two euroendocrine peptides, (a neurotensin fragment and proctolin), was measured in vitro, in the presence of tyrosinase and periodate. The authors characterized the formed dimer/trimer by UV-Vis spectrophotometry and matrix-assisted laser desorption ionization mass spectrometry. They identified the presence of di-dopa crosslinks based on the absorbance peak at 410 nm of the dimer/trimer and a weight loss of 2 Da during each coupling of dopa.⁹⁵

O-quinone may also tautomerize to form α,β -dehydro derivatives of catechols, which may

further react to form crosslinks (Fig. 25). The presence of α,β -dehydro derivatives has been identified.⁹⁶⁻⁹⁸ Rzepcki and Waite studied the oxidation of N-acetyl-dopa ethyl ester (NADEE) in the presence of sodium periodate using UV-Vis spectrometry.⁹⁷ Upon oxidation, *o*-quinone formed, as evidenced by a characteristic peak at 392 nm. This quinone peak decayed, accompanied by the emergence of a peak at 320 nm, that is characteristic for the α,β -dehydro derivative of NADEE.^{96,97} α,β -dehydro derivatives may further react with other functional groups to form crosslinked networks. However, a clear mechanism is still lacking.

To summarize, as indicated in Fig. 26, *o*-quinones can undergo dismutation with catechols to form *o*-semiquinone radicals, which further can couple to form crosslinks. The kinetics of this pathway is dependent on the presence of extra oxidants. In addition, *o*-quinones may also tautomerize to form α,β -dehydro derivatives, which further react to form crosslinks.

2.3 Polydopamine formation mechanism and possible structures

Catecholamines can undergo oxidative self-polymerization under mild alkaline condition to form homopolymers^{20,99}. The most famous example is polydopamine (PDA). PDA is insoluble in water (acid, neutral and basic), and in almost all common organic solvents and can be deposited onto any type of substrate.¹⁰⁰ This versatility, together with the reactivity of catechol with other functional groups (e.g. amines, thiols) has aroused a lot of interest in different applications, such as surface modification, biomineralization, anti-fouling coatings, water purification membranes, biotechnology and biomedicine.^{20,99,101,102}

Despite the extensive applications of PDA, the molecular mechanism of formation is still ambiguous. Initially, PDA formation was believed to resemble the formation mechanism of melanin that occurs in living organisms (Fig. 27). It was proposed that the oxidation of dopamine at basic pH leads to the formation of dopamine quinone, which subsequently goes through intramolecular cyclisation to form leucodopaminechrome. The leucodopaminechrome

is further oxidized to form dopaminechrome. Thereafter, dopaminechrome rearranges to form 5,6-dihydroxyindole (DHI), which is further oxidized to form 5,6-indolequinone. DHI and 5,6-indolequinone can subsequently go through reverse dismutation reactions to form crosslinks.³¹

Bielawski and co-workers proposed that the structure of PDA is a supramolecular aggregate of monomers (consisting of mainly DHI and its dione derivatives) instead of made up of covalent bonds among dopamines (Fig. 28).¹⁰⁰ They employed a variety of solid state spectroscopic and crystallographic techniques to analyze the isolated product from the polymerization of 3-hydroxytyramine hydrochloride under aerobic conditions, in tris(hydroxymethyl)aminomethane (TRIS) buffer at pH 8.5. They proposed that the PDA is an aggregate held together by strong non-covalent forces including hydrogen bonding, π -stacking, and charge transfer.

Recently, it has also been proposed that both covalent and non-covalent interactions (Fig. 29)¹⁰³ co-contribute to PDA formation. The proposed covalent interactions are similar to the pathway stated in Fig. 27. The dopamine goes through oxidative polymerization via DHI to form a DHI-DHI dimer, or dopamine-DHI-DHI trimer conjugates, which ultimately assemble to form polymeric aggregates. D'Ischia and co-workers reported three possible components in PDA, namely uncyclized catecholamine, cyclized indole units, and novel pyrrolecarboxylic acid moieties (Fig. 30).¹⁰⁴ Moreover, the PDA has also been proven to arise from a physical, self-assembled trimer of (dopamine)₂/DHI. The trimer complex was found to be so tightly trapped within polydopamine, that it barely escapes from the dopamine complex.¹⁰³ However, Buehler and co-workers reported that a non-covalent DHI aggregate did not contribute to PDA formation.¹⁰⁵ They developed a computational model of PDA and performed nano-indentation experiments on the prepared PDA film. They found that the Young's modulus from both studies were 4.1-4.4, and 4.3-10.5 GPa, respectively. The high

Young's modulus excludes the possibility of PDA being formed from physically self-assembled aggregates. We should point out, however, that all these models have been proposed rather than fully proven.

Based on the proposed mechanisms, PDA, in analogy to eumelanin,^{106,107} can be interpreted as supramolecular aggregates assembled from the oligomers of DHI, rather than a conventionally recognized polymer. This aggregate structure of PDA, similar to eumelanin, is thought to give rise to the PDA broadband absorption spectrum and enhanced absorption intensity at the higher-energy end.¹⁰⁷ The combination of these absorption characteristics and catechol binding functionality that PDA exhibits, results in striking optical, adhesive and mechanical properties. Lu, et al. has reported a comprehensive review on the physicochemical properties and applications of PDA.²³

Parameters influencing polydopamine formation

The PDA formation is affected by several parameters, such as the dopamine concentration, buffer type, pH, the presence of oxidant, preparation method, etc. In the following, these parameters will be discussed one by one.

The starting concentration of dopamine affects the final composition of PDA. d'Ischia and co-workers studied the polymerization of dopamine at pH 8.5 in TRIS, NaHCO₃, or phosphate buffer solutions, respectively.¹⁰⁸ They found that when the quinone was generated by auto-oxidation in the presence of a high dopamine concentration (e.g. 10×10^{-3} M), the generated quinone might be efficiently trapped, yielding mainly dimers. In contrast, when the concentration of dopamine is low (e.g. 0.5×10^{-3} M), the quinone was formed more slowly, so that the quinones were less trapped. In this way, the chances for intramolecular cyclization to give DHI were increased. The degree of polymerization of the DHI indole units was also higher than those proposed from dopamine at a higher concentration (e.g. 10×10^{-3} M). Ruch and co-workers also investigated the influence of dopamine concentration on the kinetics of

polymerization deposition.¹⁰⁹ They investigated the polymerization of dopamine in TRIS buffer at pH 8.5 for different dopamine concentrations. An exponential decay function was used to describe the deposition kinetics. $d(t) = d_0 + d_{max}(1 - e^{-kt})$, in which $d(t)$ is the time-dependent film thickness of polydopamine; d_{max} is the maximal thickness, and k is the kinetic constant. They found that d_{max} increased linearly with the dopamine initial concentration in the range of 0.1-5 g/L. In the presence of dopamine at 2 g/L and at pH 8.5, the film thickness was limited to 45 nm, as observed by Lee et al. and other researchers. However, by increasing the initial dopamine concentration to 3 and 5 g/L, the film thickness limitation could be overcome. Before the film deposition reached equilibrium, the film thicknesses were already 50 (for 3 g/L) and 70 nm (for 5 g/L), respectively. The thicker films also gave a higher roughness.

The polymerization of dopamine is also influenced by the buffer that is used. When dopamine is polymerized in TRIS buffer, as indicated by ¹³C solid state NMR, the TRIS was incorporated into the polydopamine. Therefore, the intramolecular cyclization of dopamine/quinone was inhibited, which resulted in a longer reaction time (e.g. 72h) but led to the same precipitates as compared to those prepared from phosphate or hydrogen carbonate buffers.¹⁰⁸ Ruch and co-workers have also reported the incorporation of TRIS in PDA during the reaction.¹¹⁰ They ascribed this incorporation to the presence of primary amino groups. Moreover, they found that for the polymerization of dopamine at pH 8.5 in phosphate buffer, the film could reach a thickness of up to 100 nm, whereas one obtains a thickness of 45 nm in the TRIS buffer. At pH 8.5, the phosphate was predominately present in the form of HPO_4^{2-} , and could form hydrogen bonds with the hydroxyl groups of polydopamine, resulting in a film with higher thickness. In addition, the film thickness limitation in the single-step polymerization in TRIS of pH 8.5 can be overcome by using a multistep deposition.³⁴ The multistep deposition consists of an initial immersion of the substrate in a basic dopamine

solution, followed by drying the film with a nitrogen stream, and re-initiating the oxidation process of the film by immersing it back into the starting polydopamine solution. This way, the film thickness can be grown from a few nanometers to the few hundred-nanometer.

The polymerization of dopamine largely depends on the pH. Ruch reported that d_{max} and the kinetic constant in the deposition kinetics $d(t) = d_0 + d_{max}(1 - e^{-kt})$, were largely affected by pH. In the pH range of 5-8.8, the result which unfortunately featured large error bars showed that d_{max} increased with pH, and leveled off after pH 8.5, while k increased with pH in the range of 7.0-10.2 in a reproducible way.

PDA can be formed not only under mild basic conditions; the reaction can also proceed in the presence of other oxidants, such as ammonium persulfate, sodium periodate, sodium chlorate, or Cu^{2+} .¹¹¹ It has been found that the nature of the oxidant also affects PDA formation. If the dopamine was incubated under acidic conditions, no PDA could be formed.¹¹⁰ However, by adding Cu^{2+} (Cu^{2+} : dopamine molar ratio 3), the PDA film thickness grew linearly to 60 nm within 80 h. Moreover, the initial growth of the film thickness was also slower than that from PDA formation in TRIS buffer at pH 8.5. The resulting film showed different optical properties from that prepared from TRIS buffer. The UV spectra of the film using Cu^{2+} as the oxidant showed a distinct peak at 370 nm and a small peak at 320 nm. In contrast, a film prepared using O_2 as the oxidant showed a similar spectrum to that of melanin. The authors attributed these differences to local changes in the branching between adjacent DHI due to the presence of Cu^{2+} .

To summarize, dopamine undergoes oxidative self-polymerization under mild alkaline conditions to form PDA (Fig. 31). The detailed mechanism of the polymerization as well as the structure of final PDA is still under debate. In general, both covalent and non-covalent bonds are involved in the formation of PDA. The PDA formation is influenced by several factors, such as dopamine concentration, buffer type, pH, the presence of oxidant, preparation

method, etc. By tuning these parameters, the deposition thickness of PDA on various types of substrates can be optimized.

3. Role of metal ions in adhesive curing

It has been proposed that metal ions play a key role in the cross-linking process of mussel proteins and other natural systems. In mussel adhesive, iron and other metals are present at remarkably high concentrations. The content in the organisms can be 10,000 times higher than in the open sea.¹¹²⁻¹¹⁵ Holten-Andersen et al. demonstrated that in *M. galloprovincialis* mussel byssal threads iron and dopa are colocalized in the cuticle, which is the robust protective coating covering the threads (Fig. 32).¹¹⁶ The cuticle exhibits both high hardness and high extensibility.^{117,118} The colocalization of dopa and metal ions coupled with the remarkable mechanical properties of byssal threads suggest that metal ions play an important role in mussel foot cohesion. Another natural example is the marine worm *Bdelloura candida* producing a dopa-protein, which is believed to contribute to the curing of the primary, inner layer of its eggshells.^{119,120} During the hardening and darkening of the eggshell, the metal levels (e.g., iron, copper, zinc, and lead) increase, suggesting the occurrence of a metal-dependent curing process.

It has been proposed that metal ions either chelate with catechols to form coordination complexes or mediate covalent crosslinking. In section 3.1 the formation of metal-catechol coordination complexes are discussed and the influence of different parameters such as pH, catechol: metal ion ratio and ring substituents. Growing evidence supports the role of metal-mediated covalent crosslinking in both natural and synthetic systems, which is discussed in section 3.2. We will focus our discussion on iron ions, because most of the work done so far was based on iron. In section 3.3 the influence of other metal ions on catechol crosslinking will be discussed.

3.1 Fe³⁺-catechol coordination

Catecholic hydroxyls in dopa can chelate with Fe^{3+} ions to form reversible non-covalent complexes in a variety of natural organisms such as marine worm eggshells, sea squirt wound plugs, and marine mussel adhesives.¹²¹⁻¹²⁹ For instance, some microorganisms contain molecules called siderophores that contain catechols to facilitate the solubilization and transportation of iron. One important example is enterobactin, which is produced by enteric bacteria and strongly chelates with Fe^{3+} with a stability constant of 10^{49} .^{130,131}

A chelate is formed when a catechol donates a nonbonding electron pair to the iron ion. The non-covalent complexes are formed in three different modes: mono, bis and tris catechol- Fe^{3+} complexes (Fig. 33).¹²⁹ The stoichiometry of catechol- Fe^{3+} complexes seems to be controlled by pH via the deprotonation of catecholic hydroxyls. The stoichiometric transitions were measured using a catechol functionalized polyethylene glycol polymer solution with FeCl_3 in a catechol:Fe molar ratio of 3: 1. The mono catechol- Fe^{3+} complexes dominate at $\text{pH} < 5.6$, bis at $5.6 < \text{pH} < 9.1$, and tris at $\text{pH} > 9.1$ (Fig. 34).¹³² These measurements were in agreement with earlier measurements on Fe^{3+} catechol complex formation using UV-Vis spectroscopy.¹³³ The data was also corroborated by the observation from Taylor et al. that at pH 7 both bis and tris catechol- Fe^{3+} complexes were present in *Mytilus edulis* adhesive protein, mfp-1¹³⁴. Zeng et al. proposed that the complexation mode (tris, bis, or mono complex) depends on the iron concentration.¹³⁵ At low Fe^{3+} , the tris complex formed; while at high Fe^{3+} , the mono complex formed. This dependence is was in agreement with their study on the adhesion between mfp-1 films in the presence of Fe^{3+} . In the presence of low Fe^{3+} concentration (10 μM), a number of tris complexes were formed, and significant and reversible adhesion was detected when two mfp-1 layers were brought into contact and immediately separated. In contrast, at higher Fe^{3+} concentration (100 μM), only mono complexes were formed, resulting in poor adhesion.¹³⁵

It is important to note, that the solubility of Fe^{3+} is very low, especially at high pH. Therefore, to obtain bis and tris complexes in synthetic catechol functionalized polymer systems it was

necessary to prebind Fe^{3+} in mono catechol- Fe^{3+} complexes at low pH before raising pH.¹³² Analogously, it was proposed by Holten-Andersen et al. that in mussel byssal threads, Fe^{3+} is prebound in mono-dopa- Fe^{3+} complexes by mfp-1 in secretory granules at $\text{pH} \leq 5$. Upon secretion into the seawater the pH increases which could cause the spontaneous physical crosslinking by bis- and/or tris-dopa- Fe^{3+} complex formation.¹³²

The substitution groups on the catecholic aromatic ring affect the catechol- Fe^{3+} coordination by changing the pK_a values of the catechol analogues. Studies on natural siderophores have established that catechol protonation is the rate-determining step in the dissociation of Fe^{3+} -catechol complexes.¹³⁶ Catechol derivatives exhibiting higher stability constants upon chelating with Fe^{3+} also exhibit a higher proton affinity, i.e., a higher pK_a value. Therefore, when the substitution group is electron-withdrawing, e.g., $-\text{NO}_2$, it withdraws the electron density from the catechol moiety, resulting in lower pK_a values (pK_a for nitrocatechol is 6.7 and 10.3; for catechol is 9.1 and 14).¹³⁷⁻¹³⁹ Thereby, nitro-substituted catechols are easier to chelate, i.e., nitrocatechol chelates with Fe^{3+} and forms crosslinks at lower pH values than catechols. This statement is confirmed by Menyo and co-workers. They studied the crosslinking of 4-arm PEG, end-functionalized with catechol, or nitrocatechol with Fe^{3+} at pH 9. The nitrocatechol-based hydrogels, as indicated from UV-Vis spectrophotometry data, are predominately tri-coordinated, while catechol-based gels have a great number of bis-coordinated complexes.¹⁴⁰

The ability to form bis and tris catechol complexes implicates the role of iron ions as non-covalent cross-linking agents. Iron is particularly interesting, because the stability constants of bis- and tris-catechol- Fe^{3+} complexes are among the highest known for metal-ligand chelates.^{121,129,134} Single molecule force measurements showed that the catechol- Fe^{3+} bond is only slightly weaker than a covalent bond under identical loading conditions⁷¹. It was also shown that the catechol- Fe^{3+} bonds can spontaneously reform after breaking, providing intrinsic self-healing properties to the material.⁷¹

In addition, the loss of material stiffness and hardness upon metal removal (using the chelating agent ethylenediaminetetra-acetic acid (EDTA)) observed for both synthetic and natural materials is strongly suggestive of a non-covalent crosslinking role.¹⁴¹ Nevertheless, there is growing evidence that Fe^{3+} does not only lead to non-covalent complex formation, but also plays a key role in covalent crosslinking. This will be the topic of the next section.

3.2 Covalent crosslinking mediated by Fe^{3+}

Besides coordination bond formation, Fe^{3+} may also facilitate catechol oxidation, because oxidation of catechol and reduction of Fe^{3+} occur at similar potentials (~ 0.75 V)¹⁴². Upon further reaction of the oxidized catechol, covalent crosslinks may be formed. Wilker et al. proposed^{143,144} that tris dopa- Fe^{3+} complexes undergo a valence tautomerisation in which Fe^{3+} is reduced to $\text{Fe}(\text{II})$, while dopa is oxidized to semiquinone radicals (Fig. 35). The semiquinone may further react with O_2 to generate a radical species which may persist or convert to other radicals. Radical-radical coupling can occur to provide crosslinking. This mechanism is based on insights from spectroscopic studies on whole adhesive plaques performed by Wilker et al. Electron paramagnetic resonance (EPR) spectra were obtained for plaques and showed clear signals for both an organic radical species and Fe^{3+} . In addition, they collected an EPR spectrum of extracted dopa containing adhesive proteins (mfp-1 and mfp-2) before deposition and crosslinking, which displayed no significant signal. Addition of Fe^{3+} to a solution of these proteins resulted in immediate precipitation and the EPR spectrum of the precipitate indicated a radical species and a Fe^{3+} signal. They concluded that the radical found in plaques thus appeared to arise from Fe^{3+} mediated oxidation of the protein.¹¹⁴

Additional evidence for covalent crosslinking was provided by Messersmith et al.¹⁴⁵ Gel permeation chromatography (GPC) was used to provide direct evidence of Fe^{3+} mediated covalent crosslinking for catechol functionalized polyethylene glycol polymers. GPC data showed that the extent and rate of catechol-catechol covalent bond formation mediated by Fe^{3+}

were highest at low pH. In addition, at pH 9 after 24 h in the absence of Fe^{3+} larger aggregates were found than in the presence of Fe^{3+} . The authors suggested that the Fe^{3+} may stabilize catechols against auto-oxidation by coordination. The pH dependency was corroborated by treatment of the materials with a chelating agent (EDTA). The samples designed at pH 3 were stable in EDTA, while materials fabricated at pH 5, 7 and 9 almost entirely dissolved when they were exposed to EDTA. However, the rheological properties of the different materials were not completely consistent with this picture. This needs further clarification. Finally, a pH dependent dual crosslinking mechanism was proposed, with covalent catechol-catechol adducts and Fe^{3+} catechol coordination dominating at acidic and basic conditions, respectively (Fig. 36).¹⁴⁵ The presence of catechol-catechol covalent bond has been, recently, directly observed for the reaction between 3-(3,4-dihydroxyphenyl)propionic acid (DHPA) and Fe^{3+} at acidic pH using NMR.¹⁴⁶ The protection of catechol against auto-oxidation at basic pH in the presence of Fe^{3+} has also been observed for the reaction between DOPA-containing peptide (Ac-Ser-DOPA-NH₂) and Fe^{3+} . By using HPLC-MS, at pH 9, no dimers of dipeptide were detected.¹⁴⁶ As the catechol Fe^{3+} complexes are in dynamic equilibrium,¹²⁹ Xu et al. suggested that the ratio of coordination to covalent bonds may shift over time from coordination bond to covalent bonds.¹⁴⁷ The authors reported that at shorter contact times (10 min) and low Fe^{3+} concentration (10 μM), reversible interactions between catechol and Fe^{3+} were formed. This resulted in a relatively low work of adhesion between two mfp-1 coated surfaces. With longer contact times (100 min), the redox activity of Fe^{3+} facilitates catechol oxidation by one-electron oxidation, resulting in covalent bond formation and higher adhesion (20 mN/m).^{135,144} The dynamic nature of tris-complexes, i.e., the tendency to oxidize has also been observed for Al^{3+} . Different from Fe^{3+} , Al^{3+} does not have Al^{2+} state, and the one-electron oxidation does not exist. Nevertheless, it was shown that, at pH 12, the catechol-ended 4-arm PEG hydrogel changed from pure colorless (freshly prepared hydrogel) to brown in one week. This color change implies the auto-oxidation

of tris-chelated catechol under ambient conditions.^{132,140}

By combining the insights gained, a picture emerges of a dual crosslinking mechanism: in the presence of iron, catechol-containing polymers seem to cure by a combination of coordination and covalent crosslinking. By controlling the amount and distributions of both bonds excellent cohesive properties may be obtained.

3.3 Interaction between catechol and other metal ions

In addition to Fe^{3+} , catechol can also interact with other transition metal ions. Wilker used a catechol-containing model system, i.e., acetyl-alanine-dopa-threonine-proline- CONH_2 peptide, to study catechol complexation with first-row transition metals.¹²² UV-Vis spectrometry was used to track the complexation formation during base titration (pH in the range of 3 to 11). They found that low-valent metals (i.e., Cu^{2+} , Co^{2+} , Ni^{2+}) formed 1:1 and 1:2 complexes, while high-valent ions (i.e. Fe^{3+} , V^{3+} , VO^{2+}) formed 1:1, 1:2, and 1:3 complexes.¹²² This suggests that these metal ions may also contribute to the curing of dopa proteins in natural systems. The different metal-catechol complexation stoichiometry has also been reported for Fe^{3+} and V^{3+} at pH 8.¹⁴⁸ Holten-Andersen et al. investigated the complexation of catechol end-functionalized 4-arm PEG with Fe^{3+} and V^{3+} , respectively. The UV-Vis spectra and Raman spectroscopy data showed that at pH 8, Fe^{3+} interacts with catechol via bis- coordination, while V^{3+} via tri- coordination.

Hight and Wilker found that metal ions in their reduced state, i.e., Fe^{2+} , V^{3+} , or Mn^{2+} , interact with catechols to form a weak coordination bond.¹⁴⁹ The weak bonding may be enhanced by the addition of oxidants, e.g., hydrogen peroxide or sodium periodate. By adding both metal ions (reduced state) and oxidants to catechol-based derivatives, the reduced metal ions (e.g. Fe^{2+}) may first be oxidized to its oxidized state (Fe^{3+}), which further complexes with the catechols to form strong crosslinks. This enhancement due to the oxidants, as reported by Sever and Wilker, has been observed in a study on the influence of oxidants on the curing of dopa proteins in mussel

adhesive by metal ions.¹⁴⁹ They found that, by adding oxidants (H_2O_2 or NaIO_4)^{150,151}, the resulting crosslinks from Mn^{2+} , V^{3+} and Fe^{2+} showed higher penetration forces compared to that in the absence of the oxidants, indicating a higher extent of curing. They ascribed this enhanced curing due to the oxidation of Mn^{2+} , V^{3+} and Fe^{2+} to Mn^{7+} , V^{5+} , and Fe^{3+} , respectively. The enhancement has also been observed for Ga^{3+} by adding IO_4^- . However, Ga^{3+} is not redox chemistry active except under extreme conditions. Therefore, under ambient conditions, the mechanism of crosslinking enhancement for Ga^{3+} is still not understood.

4 Conclusions and Outlook

Catechol crosslinking relies on the versatile chemistry of catechols. They can react with a variety of functionalities, e.g., amines, thiols, and metal ions. A schematic overview of all reactions is shown in Fig. 37.

Catechol-containing polymers or proteins are cross-linked either by forming covalent or non-covalent bonds. In general, the covalent crosslinking pathways start from the oxidation of catechols either by oxygen, enzymes or chemical oxidants to form *o*-quinone. The formed *o*-quinone is highly reactive and electrophilic and, therefore, susceptible for reaction with nucleophiles such as thiols and amines. The reaction either proceeds through a Michael addition or a Schiff base reaction. In addition, *o*-quinone can also undergo dismutation reactions with catechols to form *o*-semiquinone, which then form di-dopa crosslinks by phenol radical coupling. In these reactions, the *o*-quinone formation has been well studied; and the presence of di-dopa crosslinks, thiol-catechol and amine-catechol adducts have been detected in either natural organisms or synthetic polymers. The reaction kinetics of these reactions are dependent on a variety of parameters such as pH, type of oxidant (e.g. enzymes or chemical oxidant), type of ring substituents on the aromatic ring on catechols and the nucleophilic strength of thiols/amines. By tuning these parameters, the reaction kinetics can be optimized. Dopa-analogues containing both catechol and free amines in one molecule, e.g.

dopamine, can undergo oxidative self-polymerization under mild conditions by intramolecular cyclization. Several mechanisms have been proposed. This process is affected by pH, dopamine concentration, type of oxidant used, etc.

In addition, catechols can also complex with metal ions (e.g., Fe(III)) by forming coordination bonds. The modes of complexation are highly dependent on the pH. At high pH (pH > 10), tris-dopa-Fe(III) is formed. At moderate pH (e.g., $6 < \text{pH} < 8$), bis-dopa-Fe(II) is formed; and at pH 5, mono-dopa-Fe(III) is formed. Fe(III) can also oxidize catechols to form *o*-quinone, which then can form crosslinks by covalent bonding. Parameters that can be tuned to optimize the (non-covalent) crosslinking are pH, concentration of metal ions, the type of metal ions, etc.

In conclusion, the chemistry of catechols is very versatile. By using simplified catechol containing models, some parameters that affect the reaction pathways have been identified. However, detailed mechanisms for the different crosslinking reactions are still lacking. Much more research is needed to better understand the secondary reactions of *o*-quinone as well as the dual function of metal ions, i.e., coordination bond formation and redox chemistry.

Acknowledgements

M.K. acknowledges the Netherlands Organization for Scientific Research (NWO) for financial support.

References

- (1) Miserez, A.; Schneberk, T.; Sun, C. J.; Zok, F. W.; Waite, J. H. *Science* **2008**, *319*, 1816.
- (2) Zhao, H.; Sun, C.; Stewart, R. J.; Waite, J. H. *Journal of Biological Chemistry* **2005**, *280*, 42938.
- (3) Yu, J.; Wei, W.; Danner, E.; Ashley, R. K.; Israelachvili, J. N.; Waite, J. H. *Nature Chemical Biology* **2011**, *7*, 588.
- (4) Floriolli, R. Y.; Langen, J.; Waite, J. H. *Marine Biotechnology* **2000**; *2*, 352.
- (5) Chandra, S.; Gonzalez de Mejia, E. *J Agr. Food Chem.* **2004**, *52*, 3583.
- (6) Korver, O.; Wilkins, C. K.; Collier, P. *J Soc. Chem. Ind. (London)* **1973**, *93*, 89.
- (7) Purr, A.; Springer, R.; Morcinek, H. *I. Rev. Int. Chocolat.*

- 1964, 19, 398.
- (8) Pilizota, V.; Subaric, D. *Food Tech. Biotech.* **1998**, 36, 219.
 - (9) Waite, J. H.; Tanzer, M. L. *Science* **1981**, 212, 1038.
 - (10) Lee, B. P.; Messersmith, P. B.; Israelachvili, J. N.; Waite, J. H. *Annu. Rev. Mater. Res.* **2011**, 41, 99.
 - (11) Waite, J. H.; Qin, X. *Biochemistry* **2001**, 40, 2887.
 - (12) Bandara, N.; Zeng, H. B.; Wu, J. P. *Journal of Adhesion Science and Technology* **2013**, 27, 2139.
 - (13) Crisp, D. J.; Walker, G.; Young, G. A.; Yule, A. B. *J. Colloid. Interface Sci.* **1985**, 104, 40.
 - (14) Ye, Q.; Zhou, F.; Liu, W. *Chemical Society Reviews* **2011**, 40, 4244.
 - (15) Burzio, L. A.; Waite, J. H. *Biochemistry* **2000**, 39, 11147.
 - (16) Yu, M.; Hwang, J.; Deming, T. J. *Journal of the American Chemical Society* **1999**, 121, 5825.
 - (17) Yamamoto, H.; Ogawa, T.; Nishida, A. *Journal of Marine Biotechnology* **1997**, 5, 133.
 - (18) Lee, H.; Lee, B. P.; Messersmith, P. B. *Nature* **2007**, 448, 338.
 - (19) Shafiq, Z.; Cui, J.; Pastor-Pérez, L.; SanMiguel, V.; Gropeanu, R. A.; Serrano, C.; del Campo, A. *Angew. Chem. Int. Ed.* **2012**, 51, 4332.
 - (20) Lee, H.; Dellatore, S. M.; Miller, W. M.; Messersmith, P. B. *Science* **2007**, 318, 426.
 - (21) Dreyer, D. R.; Miller, D. J.; Freeman, B. D.; Paul, D. R.; Bielawski, C. W. *Chemical Science* **2013**, 4, 3796.
 - (22) Lynge, M. E.; van der Westen, R.; Postma, A.; Stadler, B. *Nanoscale* **2011**, 3, 4916.
 - (23) Liu, Y.; Ai, K.; Lu, L. *Chemical Reviews* **2014**.
 - (24) Sedo, J.; Saiz-Poseu, J.; Busque, F.; Ruiz-Monlina, D. *Adv. Mater.* **2013**, 25, 653.
 - (25) Faure, E.; Falentin-Daudré, C.; Jérôme, C.; Lyskawa, J.; Fournier, D.; Woisel, P.; Detrembleur, C. *Progress in Polymer Science* **2013**, 38, 236.
 - (26) Waite, J. H. *Comp. Biochem. Physiol.* **1990**, 97B, 19.
 - (27) Nagai, A.; Yamamoto, H. *Bull. Chem. Soc. Jpn.* **1989**, 62, 2410.
 - (28) Yamamoto, H.; Kuno, S.; Nagai, A.; Nishida, A.; Yamauchi, S.; Ikeda, K. *Int. J. Biol. Macromol.* **1990**, 12, 305.
 - (29) Bittner, S. *Amino Acids* **2006**, 30, 205.
 - (30) Wagreich, H.; Nelson, J. M. *J. Biol. Chem.* **1936**, 115, 459.
 - (31) Felix, C. C.; Sealy, R. C. *Journal of the American Chemical Society* **1982**, 104, 1555.
 - (32) Felix, C. C.; Sealy, R. C. *Photochemistry and Photobiology* **1981**, 34, 423.
 - (33) Yamazaki, I. *Free radicals in biology*; W. Pryor ed.; Academic Press: New York, 1977; Vol. 3.
 - (34) Wardman, P. *J. Phys. Chem. Ref. Data* **1989**, 18, 1637.
 - (35) Wood, P. M. *Trends in Biochemical Sciences* **1987**, 12, 250.
 - (36) Ilan, Y. A.; Meisel, D.; Czapski, G. *Israel J. Chem.* **1974**, 12, 891.
 - (37) McDowell, L. M.; Burzio, L. A.; Waite, J. H.; Schaefer, J. *The Journal of Biological Chemistry* **1999**, 274, 20293.
 - (38) Decker, H.; Terwilliger, N. *J. Exp. Biol.* **2000**, 203, 1777.
 - (39) Garcia-Borron, J. C.; Solano, F. *Pigment Cell Res.* **2002**, 15, 162.
 - (40) Gerdemann, C.; Eicken, C.; Krebs, B. *Acc. Chem. Res.* **2002**, 35, 183.
 - (41) Land, E. J.; Ramsden, C. A.; Riley, P. A. *Acc. Chem. Res.* **2003**, 36, 300.
 - (42) Solomon, E. I.; Lowery, M. D. *Science* **1993**, 259, 1575.
 - (43) Ramsden, C. A.; Riley, P. A. *Arkivoc* **2010**, 248.
 - (44) Asimov, I.; Dawson, C. R. *Journal of the American Chemical Society* **1950**, 72, 820.

- (45) Robinson, M. E.; McCance, R. A. *Biochem. J.* **1925**, *19*, 251.
- (46) Dawson, C. R.; Nelson, M. J. *J. Am. Chem. Soc.* **1938**, *60*, 250.
- (47) Ludwig, B. J.; Nelson, J. M. *J. Am. Chem. Soc.* **1939**, *61*, 2601.
- (48) Wright, C. I.; Mason, H. S. *J. Biol. Chem.* **1946**, *165*, 45.
- (49) Heacock, R. A. *Chem. Rev.* **1959**, *59*, 181.
- (50) Bors, W.; Saran, M.; Michael, C.; Lengfelder, E.; Fuchs, C.; Spottl, R. *Int. J. Radiat. Biol.* **1975**, *28*, 353.
- (51) Bors, W.; Michael, C.; Saran, M.; Lengfelder, E. *Biochem. Biophys. Acta* **1978**, *540*, 162.
- (52) Cooksey, C. J.; Garratt, P. J.; Land, E. J.; Pavel, S.; Ramsden, C. A.; Riley, P. A.; Smit, N. P. M. *J. Biol. Chem.* **1997**, *272*, 26226.
- (53) Danilewicz, J. C. *Am. J. Enol. Vitic.* **2003**, *54*, 73.
- (54) Yu, M.; Deming, T. J. *Macromolecules* **1998**, *31*, 4739-4745.
- (55) Zhang, L.; Wu, J. J.; Wang, Y. X.; Long, Y. H.; Zhao, N.; Xu, J. *J. Am. Chem. Soc.* **2012**, *134*, 9879.
- (56) Kalyanaraman, B.; Felix, C. C.; Sealy, R. C. *J. Biol. Chem.* **1984**, *259*, 354.
- (57) Sealy, R. C.; Puzyna, W.; Kalyanaraman, B.; Felix, C. C. *Biochimica et Biophysica Acta (BBA) - General Subjects* **1984**, *800*, 269.
- (58) Weidman, S. W.; Kaiser, E. T. *Journal of the American Chemical Society* **1966**, *88*, 5820.
- (59) Kaiser, E. T.; Weidman, S. W. *Tetrahedron Letters* **1965**, *9*, 497.
- (60) Liu, B.; Burdine, L.; Kodadek, T. *Journal of the American Chemical Society* **2006**, *128*, 15228.
- (61) Manthey, M.; Pyne, S.; Truscott, R. *Australian Journal of Chemistry* **1989**, *42*, 365.
- (62) Kutyrev, A. A. *Tetrahedron* **1991**, *47*, 8043.
- (63) Miserez, A.; Rubin, D.; Waite, J. H. *J. Biol. Chem.* **2010**, *285*, 38115.
- (64) Kramer, K. J.; Kanost, M. R.; Hopkins, T. L.; Jiang, H. B.; Zhu, Y. C.; Xu, R. D.; Kerwind, J. L.; Tureceke, F. *Tetrahedron Letters* **2001**, *57*, 385.
- (65) Christensen, A. M.; Schaefer, J.; Kramer, K. J.; Morgan, T. D.; Hopkins, T. L. *Journal of the American Chemical Society* **1991**, *113*, 6799.
- (66) Merritt, M. E.; Christensen, A. M.; Kramer, K. J.; Hopkins, T. L.; Schaefer, J. *Journal of the American Chemical Society* **1996**, *118*, 11278.
- (67) Schaefer, J.; Kramer, K. J.; Garbow, J. R.; Jacob, G. S.; Stejskal, E. O.; Hopkins, T. L.; Speirs, R. D. *Science* **1987**, *235*, 1200.
- (68) Weeks, W. W.; Campos, M. P.; Moldoveanu, S. *J. Agric. Food Chem.* **1993**, *41*, 1321.
- (69) Weeks, W. W.; Campos, M. P.; Moldoveanu, S. *J. Agric. Food Chem.* **1995**, *43*, 2247.
- (70) Nematollahi, D.; Afkhami, A.; Mosaed, F.; Rafiee, M. *Res. Chem. Intermed.* **2004**, *30*, 299.
- (71) Lee, H.; Scherer, N. F.; Messersmith, P. B. *PNAS* **2006**, *103*, 12999.
- (72) Khalafi, L.; Rafiee, M.; Shahbak, M.; Shirmohammadi, H. *Journal of Chemistry* **2012**, *2013*, 1.
- (73) Nematollahi, D.; Hesari, M. *Journal of Electroanalytical Chemistry* **2005**, *577*, 197.
- (74) Aveldaño, M. I.; Sprecher, H. *J. Biol. Chem.* **1987**, *262*, 1180.
- (75) Mason, H. S.; Peterson, E. W. *Biochimica et Biophysica Acta (BBA) - General Subjects* **1965**, *111*, 134.
- (76) Klein, R. F. X.; Bargas, L. M.; Horak, V.; Navarro, M. *Tetrahedron Letters* **1988**, *29*, 851.
- (77) Tian, Y.; Cao, Y.; Wang, Y.; Yang, W.; Feng, J. *Advanced Materials* **2013**, *25*, 2980.
- (78) Hurrell, R. F.; Finot, P. A. *Adv. Exp. Med. Biol.* **1984**, *177*, 423.
- (79) Manthey, M. K.; Pyne, S. G.; Truscott, R. J. W. *Aust. J. Chem.* **1989**, *42*, 365.

- (80) Faure, E.; Falentin-Daudré, C.; Lanero, T. S.; Vreuls, C.; Zocchi, G.; Van De Weerd, C.; Martial, J.; Jérôme, C.; Duwez, A. S.; Detrembleur, C. *Adv. Funct. Mater.* **2012**, *22*, 5271.
- (81) Yaylayan, V. A. *Food Sci Tech Res* **2003**, *9*, 1.
- (82) Saito, S.; Kawabata, J. *Journal of Agricultural and Food Chemistry* **2004**, *52*, 8163.
- (83) LaVoie, M. J.; Ostaszewski, B. L.; Weihofen, A.; Schlossmacher, M. G.; Selkoe, D. J. *Nat. Med.* **2005**, *11*, 1214.
- (84) Zhao, H.; Waite, J. H. *J. Biol. Chem.* **2006**, *281*, 26150.
- (85) Zhao, H.; Waite, J. H. *Biochemistry* **2005**, *44*, 15915.
- (86) Ohkawa, K.; Nagai, T.; Nishida, A.; Yamamoto, H. *J. Adhes.* **2009**, *85*, 770.
- (87) Brandes, N.; Schmitt, S.; Jacob, U. *Antioxid. Redox Signal* **2009**, *11*, 997.
- (88) Jensen, K. S.; Hansen, R. E.; Winther, J. R. *Antioxid. Redox Signal* **2009**, *11*, 1047.
- (89) Kim, H. S.; Ham, H. O.; Son, Y. J.; Messersmith, P. B.; Yoo, H. S. *Journal of Materials Chemistry B* **2013**, *1*, 3940.
- (90) Lee, Y. H.; Chung, H. J.; Yeo, S. H.; Ahn, C. H.; Lee, H.; Messersmith, P. B.; Park, T. G. *Soft Matter* **2010**, *6*, 977.
- (91) Nikolantonaki, M.; Jourdes, M.; Shinoda, K.; Teissedre, P.-L.; Quideau, S.; Darriet, P. *Journal of Agricultural and Food Chemistry* **2012**, *60*, 2647.
- (92) Charles-Bernard, M.; Kraehenbuehl, K.; Rytz, A.; Roberts, D. D. *Journal of Agricultural and Food Chemistry* **2005**, *53*, 4417.
- (93) Nikolantonaki, M.; Chichuc, I.; Teissedre, P.-L.; Darriet, P. *Analytica Chimica Acta* **2010**, *660*, 102.
- (94) Haemers, S.; Koper, G. J. M.; Frens, G. *Biomacromolecules* **2003**, *4*, 632.
- (95) Burizio, L. A.; Waite, J. H. *Protein Science* **2001**, *10*, 735.
- (96) Sugumaran, M. *Adv. Insect Phys.* **1998**, *27*, 230.
- (97) Rzepecki, L. M.; Waite, J. H. *Arch. Biochem. Biophys.* **1991**, *285*, 27.
- (98) Lee, B. P.; Dalsin, J. L.; Messersmith, P. B. *Biomacromolecules* **2002**, *3*, 1038.
- (99) Kang, S. M.; Rho, J. S.; Choi, I. S.; Messersmith, P. B.; Lee, H. *J. AM. CHEM. SOC.* **2009**, *131*, 13224.
- (100) Dreyer, D. R.; Miller, D. J.; Freeman, B. D.; Paul, D. R.; Bielawski, C. W. *Langmuir* **2012**, *28*, 6428.
- (101) Lee, H.; Rho, J. S.; Messersmith, P. B. *Adv. Mater.* **2009**, *21*, 431.
- (102) Xu, L. Q.; Yang, W. J.; Neoh, K. G.; Kang, E. T.; Fu, G. D. *Macromolecules* **2010**, *43*, 8336.
- (103) Hong, S.; Na, Y. S.; Choi, S.; Song, I. T.; Kim, W. Y.; Lee, H. *Adv. Funct. Mater.* **2012**, *22*, 4711.
- (104) Vecchia, N. F. D.; Avolio, R.; Alfè, M.; Errico, M. E.; Napolitano, A.; d'Ischia, M. *Adv. Funct. Mater.* **2013**, *23*, 1331.
- (105) Lin, S. C.; Chen, C. T.; Bdikin, I.; Ball, V.; Graciob, J.; Buehler, M. J. *Soft Matter* **2014**, *10*, 457.
- (106) Chen, C. T.; Ball, V.; de Almeida Gracio, J. J.; Singh, M. K.; Toniazzi, V.; Ruch, D.; Buehler, M. J. *ACS Nano* **2013**, *7*, 1524.
- (107) Chen, C.-T.; Chuang, C.; Cao, J.; Ball, V.; Ruch, D.; Buehler, M. J. *Nature Communications* **2014**, *5*, 3839.
- (108) Della Vecchia, N. F.; Avolio, R.; Alfè, M.; Errico, M. E.; Napolitano, A.; d'Ischia, M. *Advanced Functional Materials* **2013**, *23*, 1331.
- (109) Ball, V.; Frari, D. D.; Toniazzi, V.; Ruch, D. *Journal of Colloid and Interface Science* **2012**, *386*, 366.
- (110) Bernsmann, F.; Ball, V.; Addiego, F. d. r.; Ponche, A.; Michel, M.; Gracio, J. J. d. A.; Toniazzi, V. r.; Ruch, D. *Langmuir* **2011**, *27*, 2819.
- (111) Wei, Q.; Zhang, F.; Li, J.; Li, B.; Zhao, C. *Polymer Chemistry* **2010**, *1*, 1430.

- (112) Coombs, T. L.; Keller, P. J. *Aquat Toxicol* **1981**, *1*, 291.
- (113) Rzepecki, L. M.; Waite, J. H. *Bioorganic marine chemistry*; Springer-Verlag: New York, 1991.
- (114) Sever, M. J.; Weisser, J. T.; Monahan, J.; Srinivasan, S.; Wilker, J. J. *Angew Chem Int Ed* **2004**, *43*, 448.
- (115) George, S. G.; Pirie, B. J. S.; Coombs, T. L. *J. Exp. Mar. Bio. Ecol.* **1976**, *23*, 71.
- (116) Holten-Andersen, N.; Mates, T. E.; Toprak, M. S.; Stucky, G. D.; Zok, F. W.; Waite, J. H. *Langmuir* **2009**, *25*, 3323.
- (117) Holten-Andersen, N.; Fantner, G. E.; Hohlbauch, S.; Waite, J. H.; Zok, F. W. *Nat. Mater.* **2007**, *6*, 669.
- (118) Harrington, M. J.; Masic, A.; Holten-Andersen, A.; Waite, J. H.; Fratzl, P. *Science* **2010**, *328*, 216.
- (119) Swann, C. P.; Waite, J. H.; Huggins, L. G. *Nucl. Instrum. Methods Phys. Res., Sect. B* **1996**, *109/110*, 301.
- (120) Huggins, L. G.; Waite, J. H. *J. Exp. Zool.* **1993**, *265*, 549.
- (121) Taylor, S. W.; Luther III, G. W.; Waite, J. H. *Inorg. Chem.* **1994**, *33*, 5819.
- (122) Sever, M. J.; Wilker, J. J. *Dalton Trans.* **2006**, 813.
- (123) Dorsett, L. C.; Hawkins, C. J.; Grice, J. A.; Lavin, M. F.; Merefield, P. M.; Parry, D. L.; Ross, I. L. *Biochemistry* **1987**, *26*, 8078.
- (124) Oltz, E. M.; Bruening, R. C.; Smith, M. J.; Kustin, K.; Nakanishi, K. *J. Am. Chem. Soc.* **1988**, *110*, 6162.
- (125) Taylor, S. W.; Hawkins, C. J.; Winzor, D. J. *Inorg. Chem.* **1993**, *32*, 422.
- (126) Taylor, S. W.; Ross, M. M.; Waite, J. H. *Arch. Biochem. Biophys.* **1995**, *324*, 228.
- (127) Smith, M. J.; Ryan, D. E.; Nakanishi, K.; Frank, P.; Hodgson, K. *O. Met. Ions Biol. Syst.* **1995**, *31*, 423.
- (128) Taylor, S. W.; Kammerer, B.; Bayer, E. *Chem. Rev.* **1997**, *97*, 333.
- (129) Avdeef, A.; Sofen, S. R.; Bregante, T. L.; Raymond, K. N. *J. Am. Chem. Soc.* **1978**, *100*, 5362.
- (130) Dertz, E. A.; Raymond, K. N. *Comprehensive coordination chemistry II*; Elsevier Pergamon: Boston, 2003; Vol. 8.
- (131) Loomis, L. D.; Raymond, K. N. *Inorg. Chem.* **1991**, *30*, 906.
- (132) Holten-Andersen, N.; Harrington, M. J.; Birkedal, H.; Lee, B. P.; Messersmith, P. B.; Lee, K. Y. C.; Waite, J. H. *PNAS* **2011**, *108*, 2651.
- (133) Severa, M. J.; Wilker, J. J. *Dalton Trans.* **2004**, 1061.
- (134) Taylor, S. W.; Chase, D. B.; Emptage, M. H.; Nelson, M. J.; Waite, J. H. *Inorg. Chem.* **1996**, *35*, 7572.
- (135) Zeng, H. B.; Hwang, D. S.; Israelachvili, J. N.; Waite, J. H. *PNAS* **2010**, *107*, 12850.
- (136) Monzyk, B.; Crumbliss, A. L. *J Am. Chem. Soc.* **1982**, *104*, 4912.
- (137) Nurchi, V. M.; Pivetta, T.; Lachowicz, J. I.; Crisponi, G. J. *Inorg. Biochem.* **2009**, *103*, 227.
- (138) Burgess, J.; Rangel, M. *Adv. Inorg. Chem.* **2008**, *60*, 167.
- (139) Zhou, T.; Ma, Y.; Kong, X.; Hider, R. C. *Dalton Trans.* **2012**, *41*, 6371.
- (140) Menyo, M. S.; Hawker, C. J.; Waite, J. H. *Soft Matter* **2013**, *9*, 10314.
- (141) Broomell, C. C.; Mattoni, M. A.; Zok, F. W.; Waite, J. H. *J. Exp. Biol.* **2006**, *209*, 3219.
- (142) Kipton, H.; Powell, J. *Aust. J. Chem.* **1982**, *35*, 739.
- (143) Wilker, J. J. *Curr. Opin. Chem. Biol.* **2010**, *14*, 276.
- (144) Monahan, J.; Wilker, J. J. *Chemical Communications* **2003**, 1672.
- (145) Barrett, D. G.; Fullenkamp, D. E.; He, L. H.; Holten-Andersen, N.; Lee, K. Y. C.; Messersmith, P. B. *Adv. Funct. Mater.* **2013**, *23*, 1111.
- (146) Fullenkamp, D. E.; Barrett, D. G.; Miller, D. R.; Kurutz, J. W.; Messersmith, P. B. *RSC Adv.* **2014**, *4*, 25127.
- (147) Xu, H.; Nishida, J.; Ma, W.; Wu, H.; Kobayashi, M.; Otsuka, H.; Takahara, A. *ACS Macro Lett.* **2012**, *1*, 457.

- (148) Holten-Andersen, N.; Jaishankar, A.; Harrington, M. J.; Fullenkamp, D. E.; DiMarco, G.; He, L. H.; McKinley, G. H.; Messersmith, P. B.; Lee, K. Y. C. *J. Mater. Chem. B* **2014**, *2*, 2467.
- (149) Sever, M. J.; Wilker, J. J. *J Mater. Sci.* **2007**, *42*, 8934.
- (150) Lide, D. R. *CRC handbook of chemistry and physics*; CRC Press: Boca Raton, 1992.
- (151) Bratsch, S. G. *J. Phys. Chem. Ref. Data* **1989**, *18*, 1.
- (152) Kalyanaraman, B.; Felix, C. C.; Sealy, R. C. *Environmental Health Perspectives* **1985**, *64*, 185.
- (153) Decker, H.; Tuzcek, F. *Trends Biochem. Sci.* **2000**, *25*, 392.
- (154) Inaba, K. *Genes to cells* **2010**, *15*, 935.
- (155) Yu, F.; Chen, S. G.; Chen, Y.; Li, H. M.; Yang, L. J.; Chen, Y. Y.; Yin, Y. S. *Journal of Molecular Structure* **2010**, 982 152.

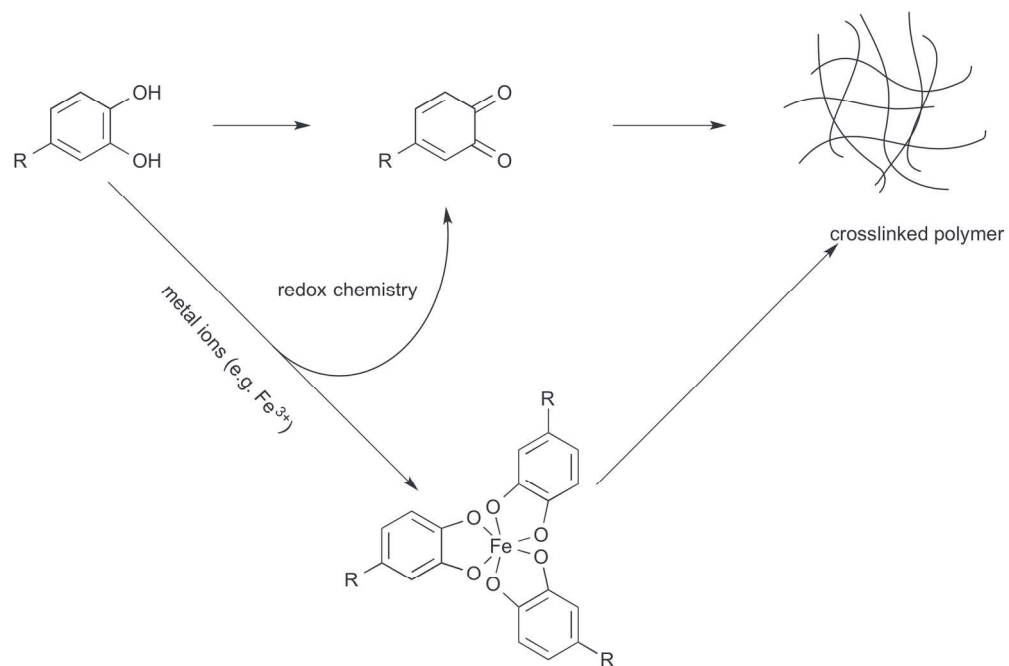


Figure 1. General crosslinking pathways of catechols
83x55mm (600 x 600 DPI)

Figure captions

Figure 1. General crosslinking pathways of catechols

Figure 2. Reaction scheme of auto-oxidation of catechol to *o*-quinone¹⁵²

Figure 3. View of the structure of tyrosinase around the oxygen-binding site of *Limulus polyphemus* hemocyanin, as based on the X-ray structure.¹⁵³ Reprinted from ref. 153, Copyright 2000, with permission from Elsevier.

Figure 4. Activation of tyrosinase for catechol oxidation⁴¹

Figure 5. Oxidation mechanism of catechol catalyzed by tyrosinase.⁴¹ Step 2 is identical to step 3 in Fig. 2.

Figure 6. Catecholic oxidation cycle mediated by tyrosinase⁴¹

Figure 7. Competing oxidase (k_1) and inactivation (k_2) reactions of tyrosinase⁴³

Figure 8. Proposed pathways of decomposition of the intermediate to form *o*-quinone.⁵⁸

Figure 9. Reaction mechanism of *p*-quinone with primary amines through Michael-type addition⁶²

Figure 10. Crosslinks identified in *D. gigas* squid beak by MS/MS, the structures are (a) 4-methylcatechol-histidine (4MC-His); (b) dopa-histidine; (c) 4MC-his-4MC; (d) His-4MC-His; (e) 4MC-His-dopa; (f) His-4MC-His-4MC⁶³

Figure 11. Proposed crosslinking pathway for sclerotization.⁶⁴ Reprinted from ref. 64, Copyright 2001, with permission from Elsevier.

Figure 12. Proposed crosslink structure for sclerotized insect cuticle involving N- β -alanyldopamine.⁶⁵

Figure 13. Reaction of *o*-quinone with nornicotine.²⁹ Reprinted from ref. 29, Copyright 2004, with permission from Springer.

Figure 14. Reaction scheme of catechol with sulfanilic acid.⁷⁰ Reprinted from ref. 70, Copyright 2006, with permission from Springer.

Figure 15. Michael addition reaction products from reaction of aniline and *o*-quinone; (a) 4,5-diarylamino-1,2-dihydrobenzene (b) and (c) tautomers of 4,5-diarylamino-1,2-dihydrobenzene. d) Product from Schiff base reaction.⁷⁹

Figure 16. Reaction mechanism of catechol/4-methyl catechol with *N*-methylaniline⁷²

Figure 17. Reaction scheme of 3,4-di-*tert*-butyl-1,2-benzoquinone with cyclohexylamine⁷⁶

Figure 18. Reaction mechanism of catechol with 2-phenylethylamine under a) neutral pH; b) high pH (11.7)⁷⁹

Figure 19. Strecker degradation reaction

Figure 20. *o*-quinone reaction with amines

Figure 21. Proposed mechanism for the conjugation of catechol to a nucleophilic thiol group in aprotic solvent⁸²

Figure 22. Proposed reaction mechanism of quinone reduction by thiolates.¹⁵⁴ Reprinted from ref. 154, Copyright 2011, by permission from Macmillan Publishers Ltd.

Figure 23. Michael type addition of catechols with thiols

Figure 24. Crosslinking pathways by aryloxyl coupling

Figure 25. Tautomerization of *o*-quinone to α,β -dehydro derivative

Figure 26. *o*-quinone forms crosslinks via two pathways: dismutation and tautomerization

Figure 27. Reaction mechanism of melanin formation by dopamine oxidation.¹⁵⁵ Reproduced with permission from ref. 155. Copyright 2013, WILEY-VCH Verlag GmbH & Co. KGaA, Weinheim.

Figure 28. The PDA material is proposed to be comprised of intra- and interchain noncovalent interactions, including hydrogen bonding, π -stacking, and charge transfer.¹⁰⁰ Reprinted from ref. 100, Copyright 2010, with permission from Elsevier.

Figure 29. Polydopamine synthesis occurs via two pathways.¹⁰³ Reprinted with permission from ref. 103. Copyright (1982) American Chemical Society.

Figure 30. Simplified overall view of main reaction pathways involved in polydopamine formation.¹⁰⁴ Reproduced with permission from ref. 104. Copyright 2012, WILEY-VCH Verlag GmbH & Co. KGaA, Weinheim.

Figure 31. Polydopamine formation

Figure 32: Maps of Fe, Ca, N, and C distributions in a transverse cross-section of a mussel thread generated using secondary ion mass spectroscopy (SIMS).¹¹⁶ Reprinted with permission from ref. 116. Copyright (2009) American Chemical Society

Figure 33: pH dependent stoichiometry of Fe^{3+} .¹³²

Figure 34: Catechol functionalized polyethylene glycol polymer. Relative fractions of mono bis and tris catechol- Fe^{3+} complexes in solutions with catechol-PEG with FeCl_3 (catechol: Fe molar ratio of 3:1) as a function of pH.¹³²

Figure 35. Proposed mechanism of iron mediated catechol crosslinking.¹⁴³ Reprinted from ref. 143, Copyright 2010, with permission from Elsevier.

Figure 36: Proposed pH dependence of covalent and coordination bond formation mediated by Fe^{3+} in catechol functionalized polymers.¹⁴⁵ Reproduced with permission from ref. 145. Copyright 2013, WILEY-VCH Verlag GmbH & Co. KGaA, Weinheim.

Figure 37. Crosslinking pathways of catechol-containing proteins

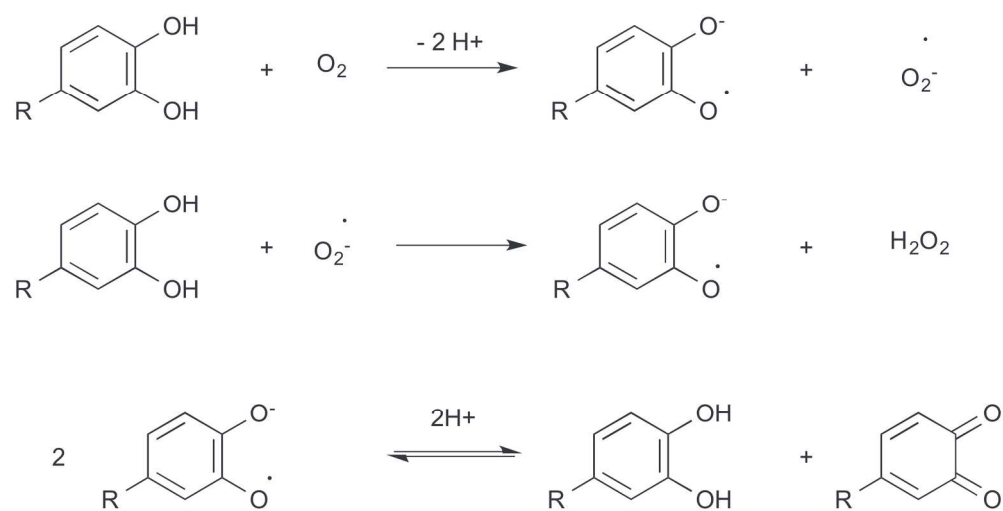


Figure 2. Reaction scheme of auto-oxidation of catechol to o-quinone¹⁵²
95x90mm (600 x 600 DPI)

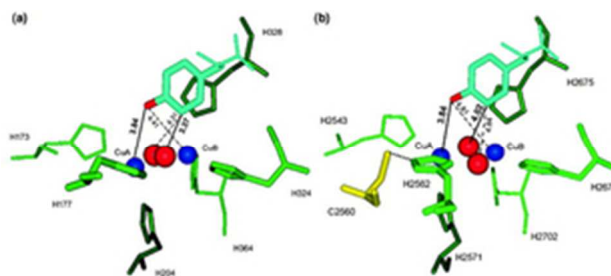


Figure 3. View of the structure of tyrosinase around the oxygen-binding site of *Limulus polyphemus* hemocyanin, as based on the X-ray structure.¹⁵³ Reprinted from ref. 153, Copyright 2000, with permission from Elsevier.
26x11mm (300 x 300 DPI)

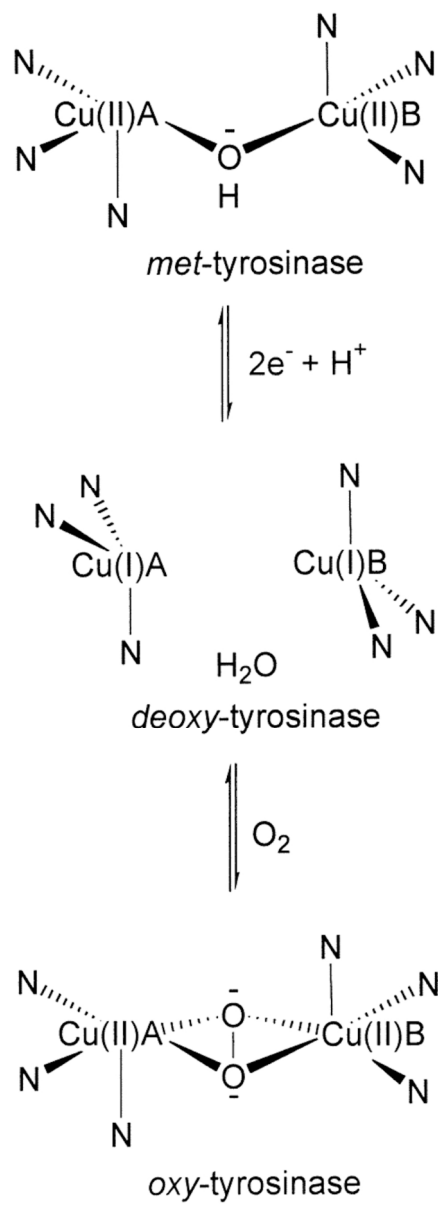


Figure 4. Activation of tyrosinase for catechol oxidation⁴¹
83x230mm (300 x 300 DPI)

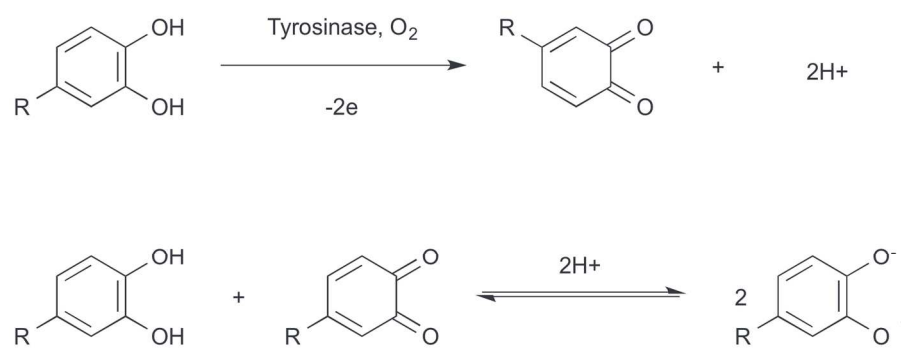


Figure 5. Oxidation mechanism of catechol catalyzed by tyrosinase.⁴¹ Step 2 is identical to step 3 in Fig. 2.
84x66mm (600 x 600 DPI)



Figure 6. Catecholic oxidation cycle mediated by tyrosinase⁴¹
17x6mm (300 x 300 DPI)

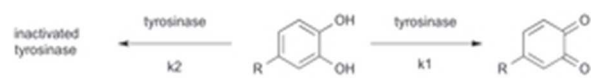


Figure 7. Competing oxidase (k1) and inactivation (k2) reactions of tyrosinase⁴³
12x1mm (600 x 600 DPI)

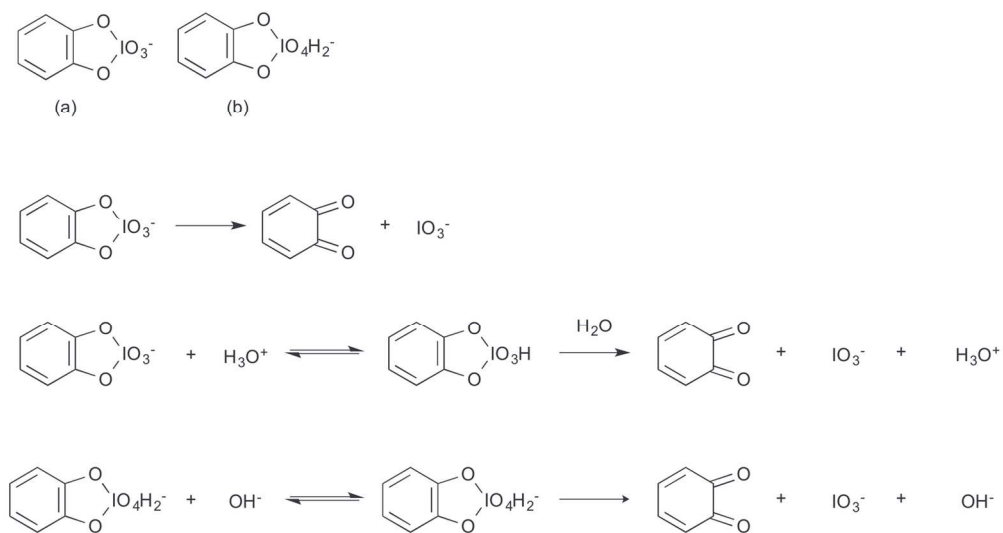


Figure 8. Proposed pathways of decomposition of the intermediate to form o-quinone.⁵⁸
71x38mm (600 x 600 DPI)

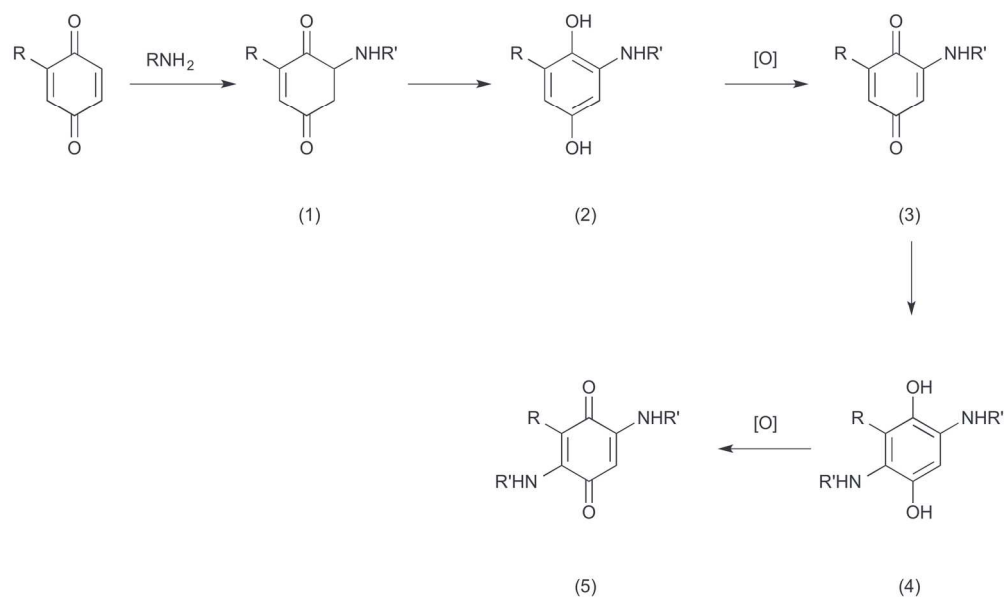


Figure 9. Reaction mechanism of p-quinone with primary amines through Michael-type addition⁶²
80x47mm (600 x 600 DPI)

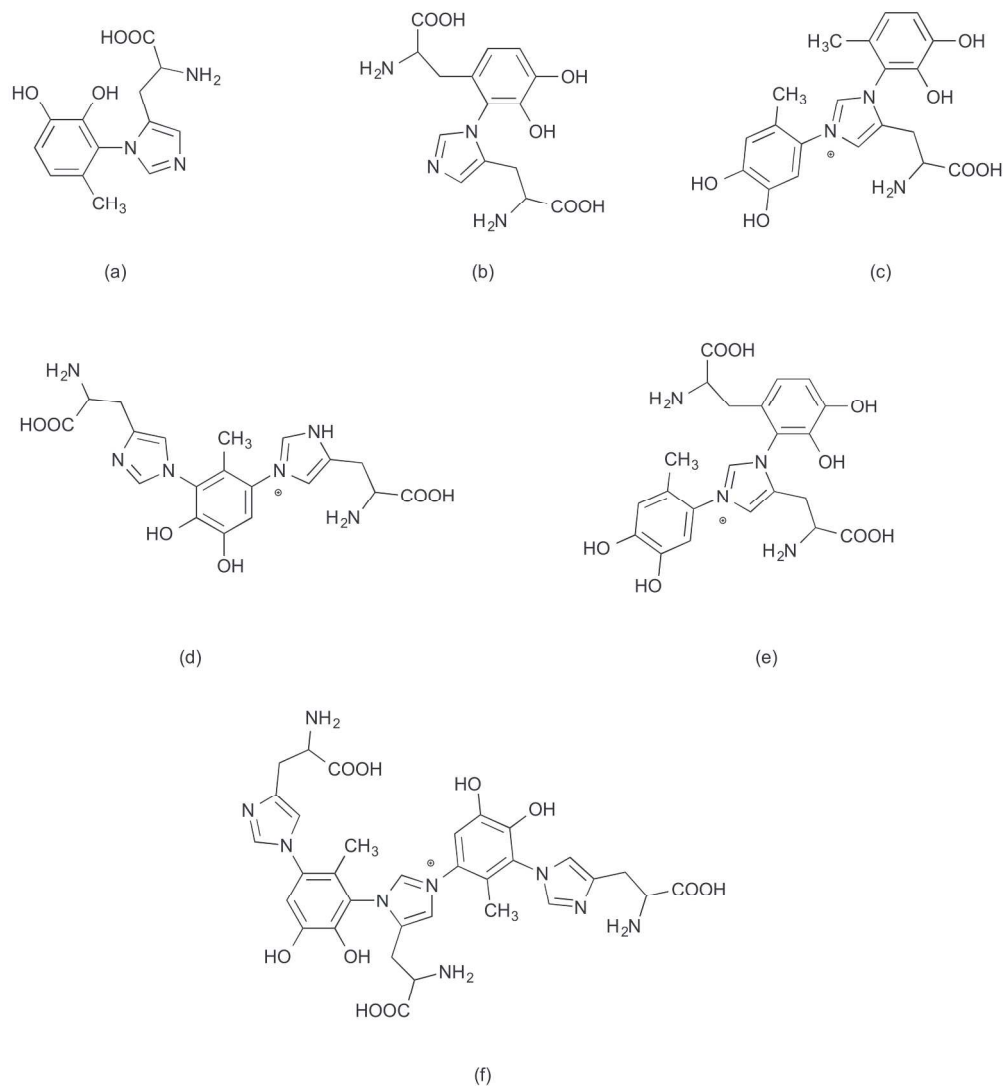


Figure 10. Crosslinks identified in *D. gigas* squid beak by MS/MS, the structures are (a) 4-methylcatechol-histidine (4MC-His); (b) dopa-histidine; (c) 4MC-his-4MC; (d) His-4MC-His; (e) 4MC-His-dopa; (f) His-4MC-His-4MC⁶³
145x157mm (600 x 600 DPI)

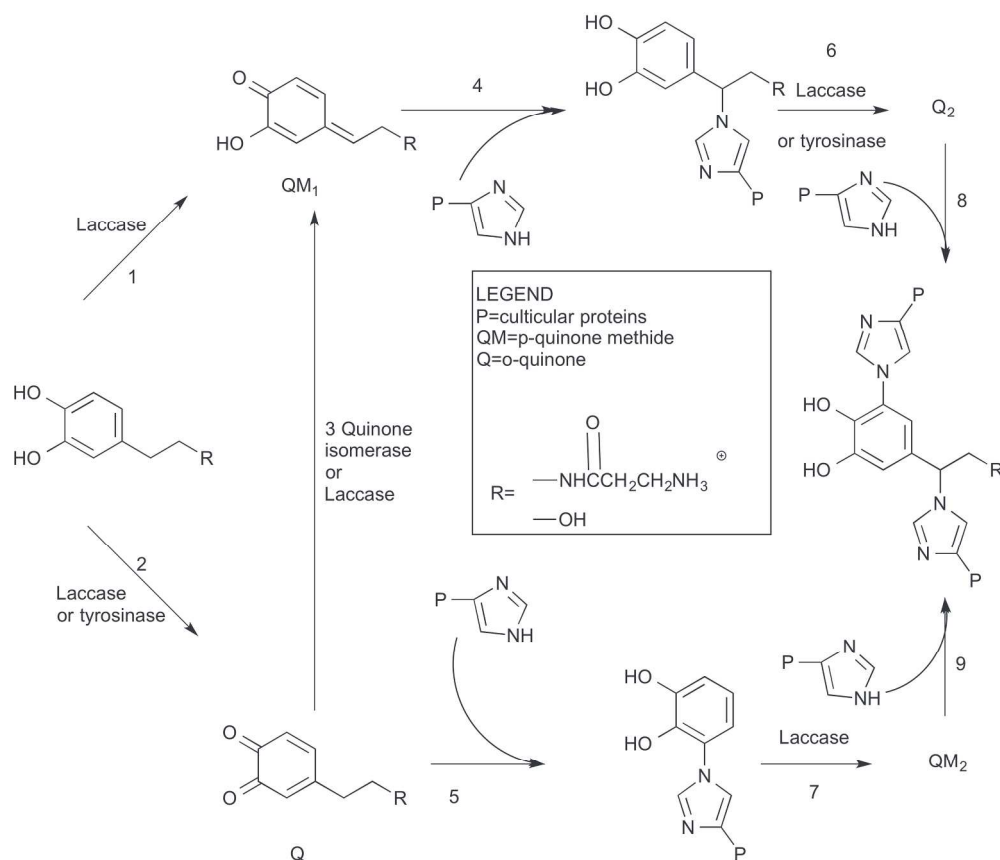


Figure 11. Proposed crosslinking pathway for sclerotization.⁶⁴ Reprinted from ref. 64, Copyright 2001, with permission from Elsevier.
112x96mm (600 x 600 DPI)

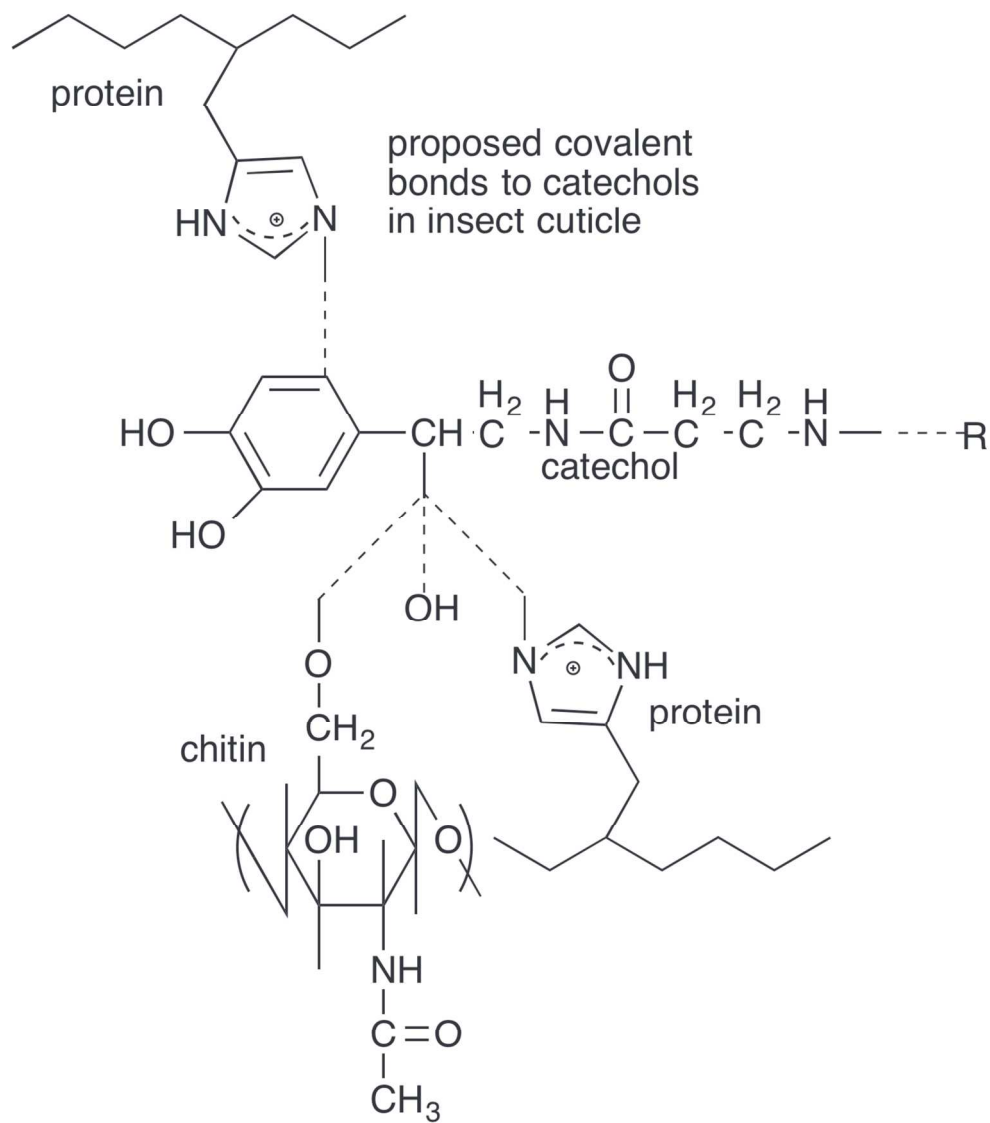


Figure 12. Proposed crosslink structure for sclerotized insect cuticle involving N-β-alanyldopamine.⁶⁵
74x84mm (600 x 600 DPI)

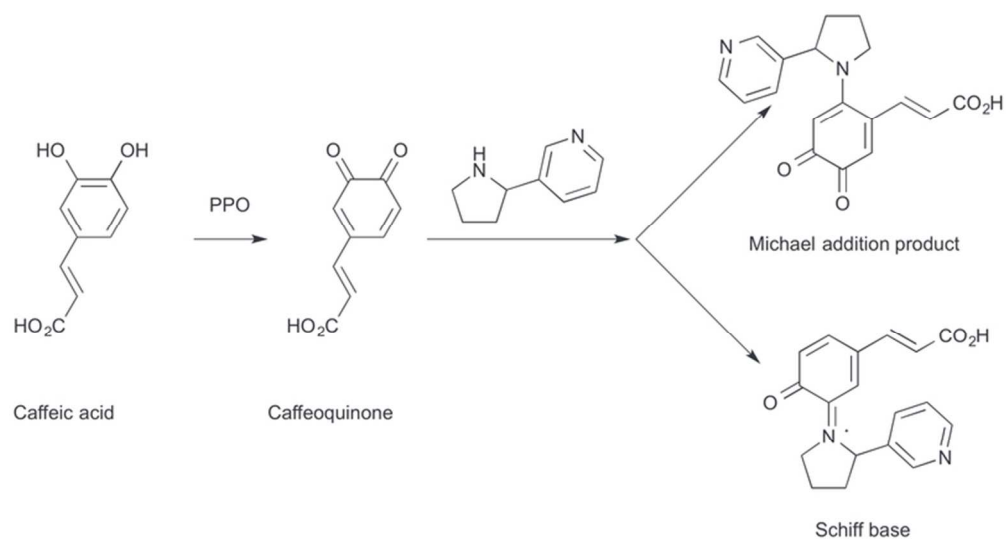


Figure 13. Reaction of o-quinone with nornicotine.²⁹ Reprinted from ref. 29, Copyright 2004, with permission from Springer.
68x36mm (300 x 300 DPI)

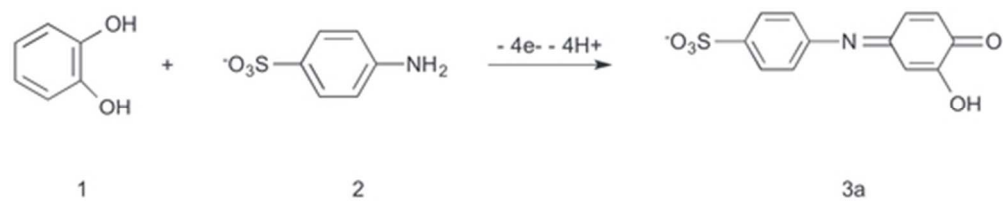


Figure 14. Reaction scheme of catechol with sulfanilic acid.⁷⁰ Reprinted from ref. 70, Copyright 2006, with permission from Springer.
22x4mm (600 x 600 DPI)

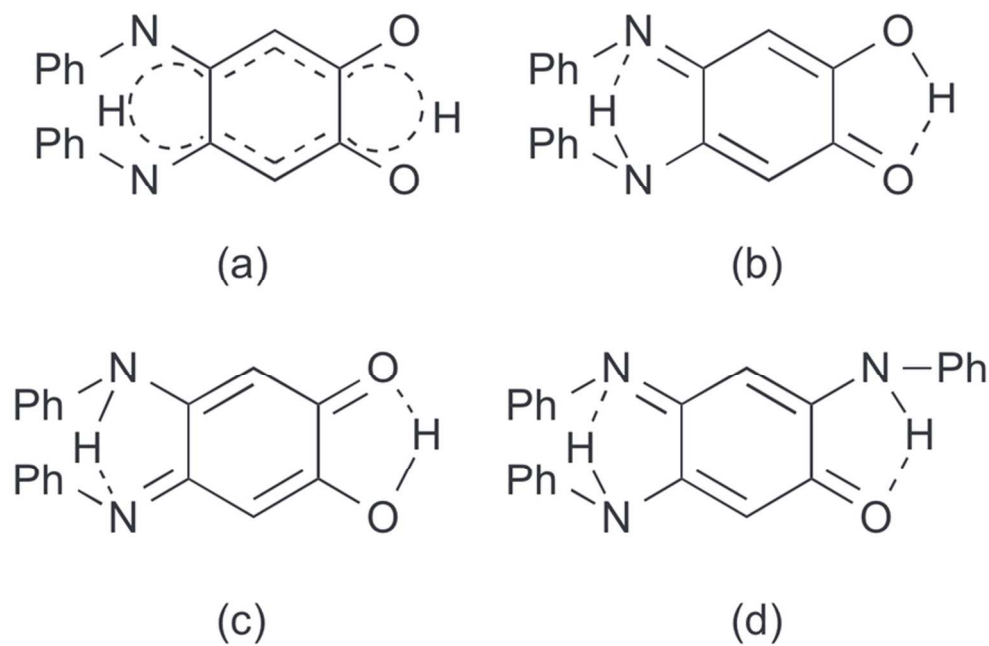


Figure 15. Michael addition reaction products from reaction of aniline and o-quinone; (a) 4,5-diarylamino-1,2-dihydrobenzene (b) and (c) tautomers of 4,5-diarylamino-1,2-dihydrobenzene. d) Product from Schiff base reaction.⁷⁹

38x25mm (600 x 600 DPI)

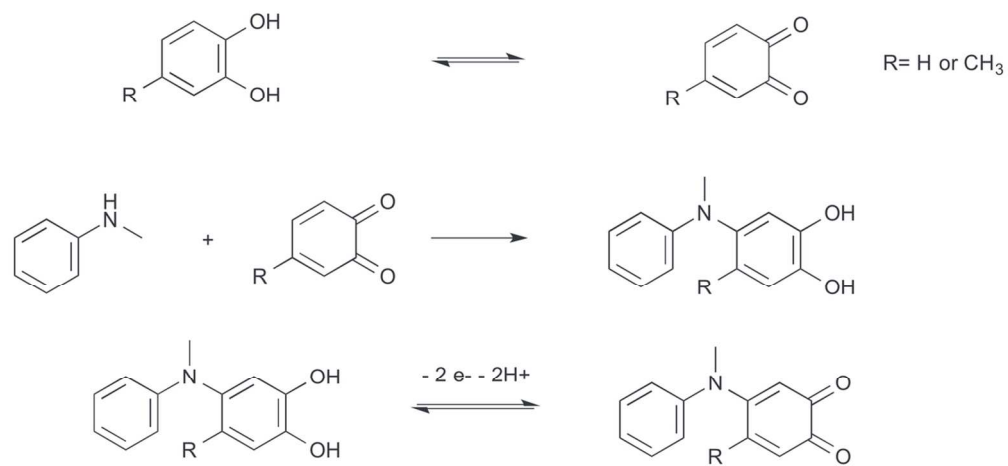


Figure 16. Reaction mechanism of catechol/4-methyl catechol with N-methylaniline⁷²
54x25mm (600 x 600 DPI)

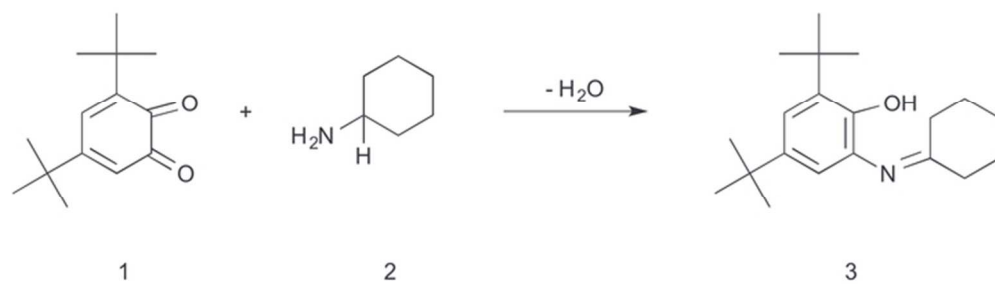


Figure 17. Reaction scheme of 3,4-di-*tert*-butyl-1,2-benzoquinone with cyclohexylamine⁷⁶
30x8mm (600 x 600 DPI)

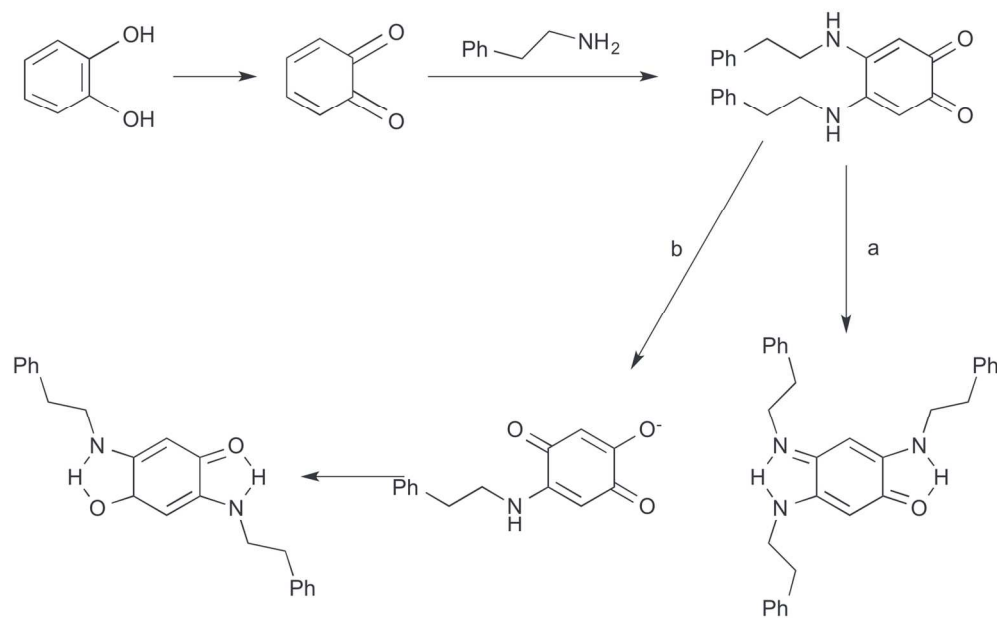


Figure 18. Reaction mechanism of catechol with 2-phenylethylamine under a) neutral pH; b) high pH (11.7)⁷⁹
69x42mm (600 x 600 DPI)

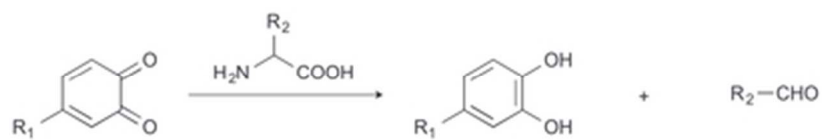


Figure 19. Strecker degradation reaction
17x2mm (600 x 600 DPI)

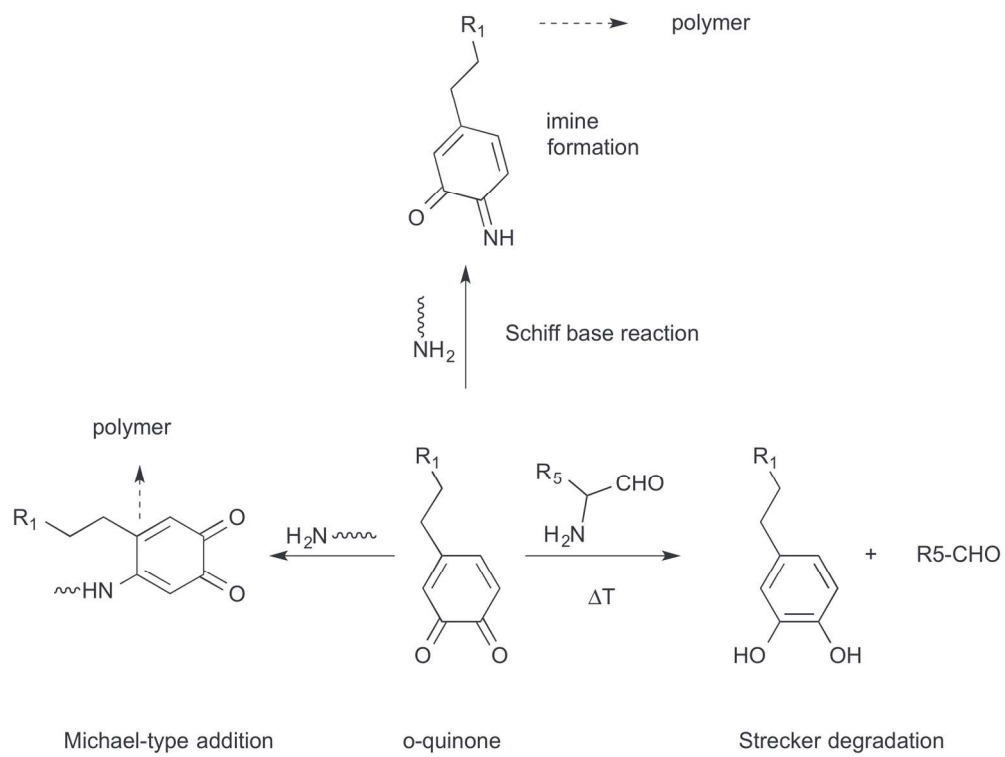


Figure 20. *o*-quinone reaction with amines
84x63mm (600 x 600 DPI)

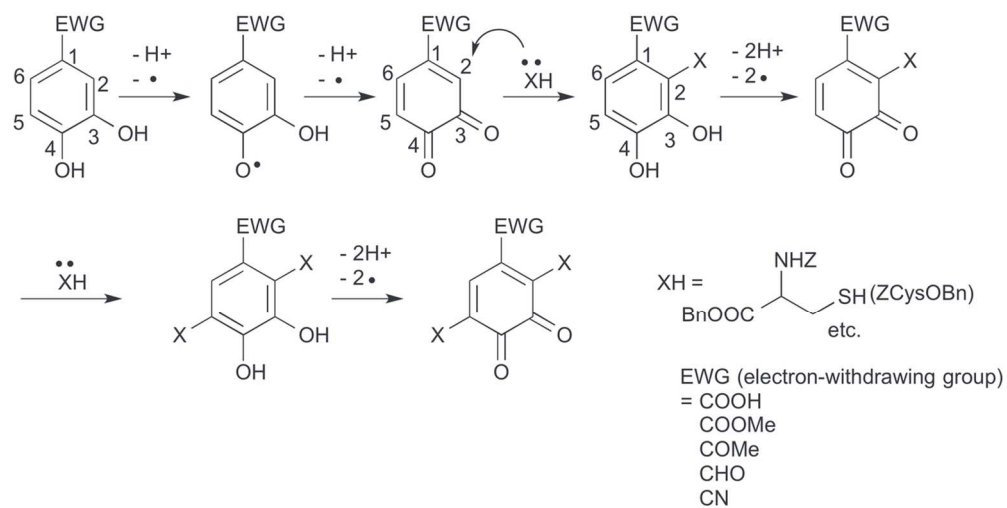


Figure 21. Proposed mechanism for the conjugation of catechol to a nucleophilic thiol group in aprotic solvent⁸²
 59x30mm (600 x 600 DPI)

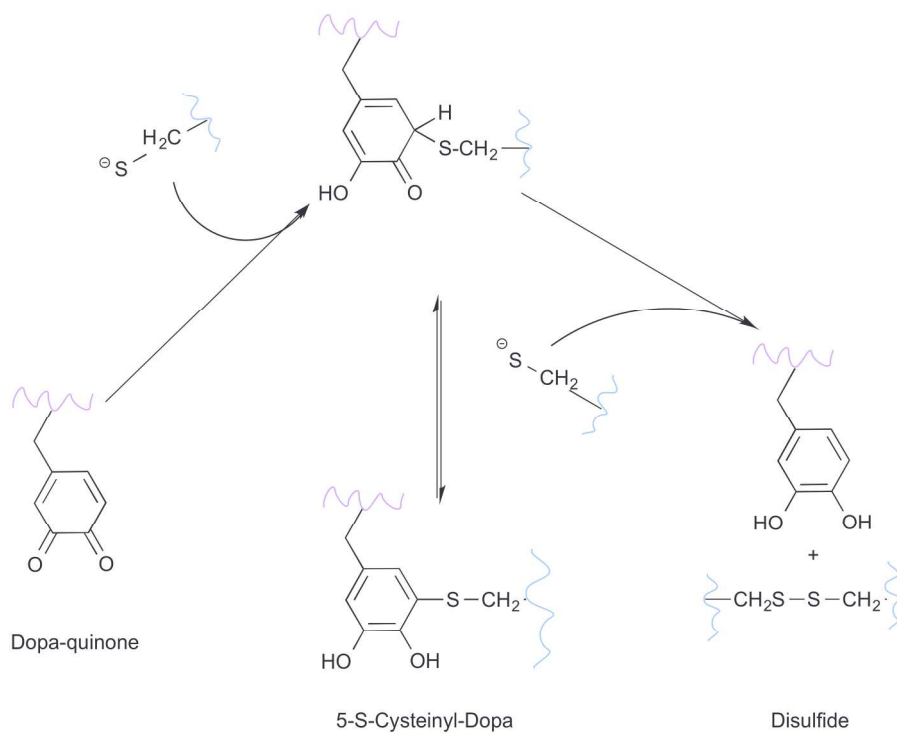
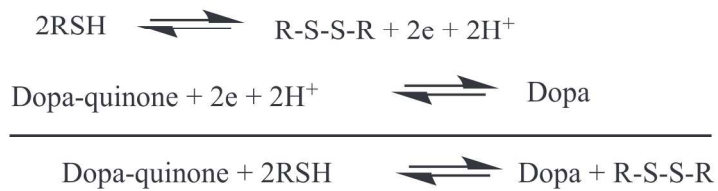


Figure 22. Proposed reaction mechanism of quinone reduction by thiolates.¹⁵⁴ Reprinted from ref. 154, Copyright 2011, by permission from Macmillan Publishers Ltd. 142x167mm (600 x 600 DPI)

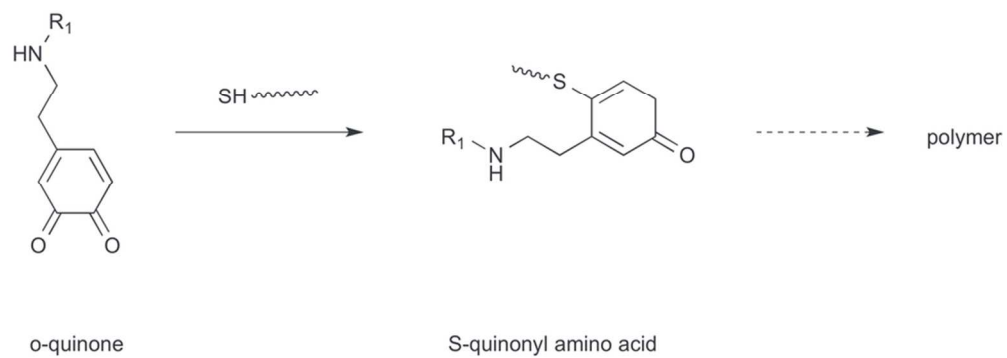


Figure 23. Michael type addition of catechols with thiols
41x14mm (600 x 600 DPI)

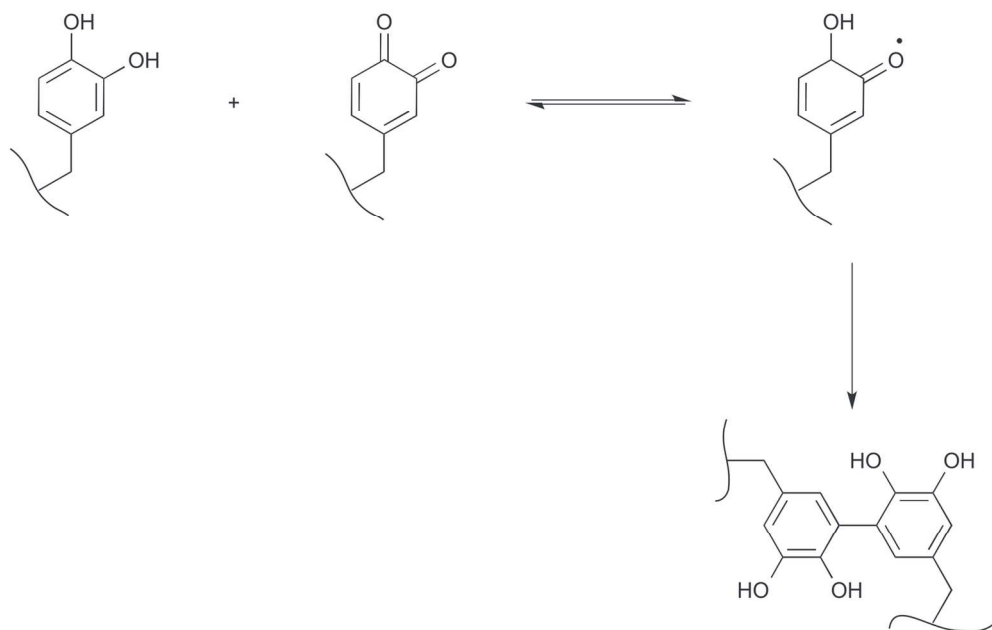


Figure 24. Crosslinking pathways by aryloxy coupling
72x45mm (600 x 600 DPI)

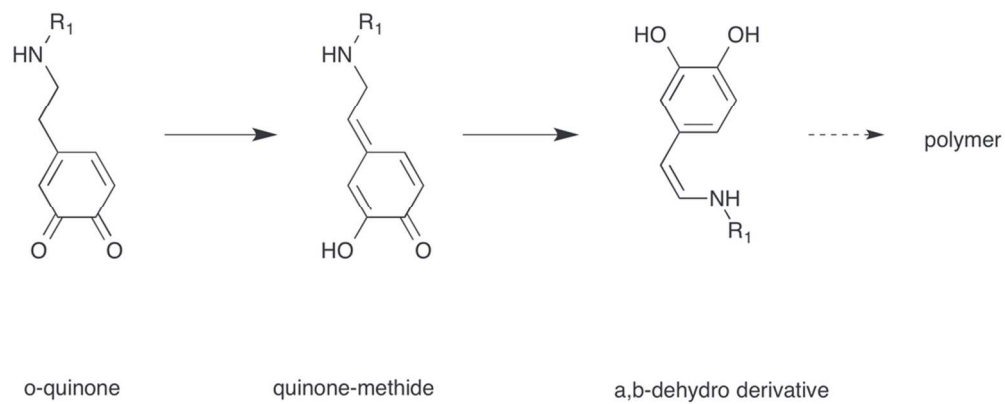


Figure 25. Tautomerization of *o*-quinone to α,β -dehydro derivative
45x18mm (600 x 600 DPI)

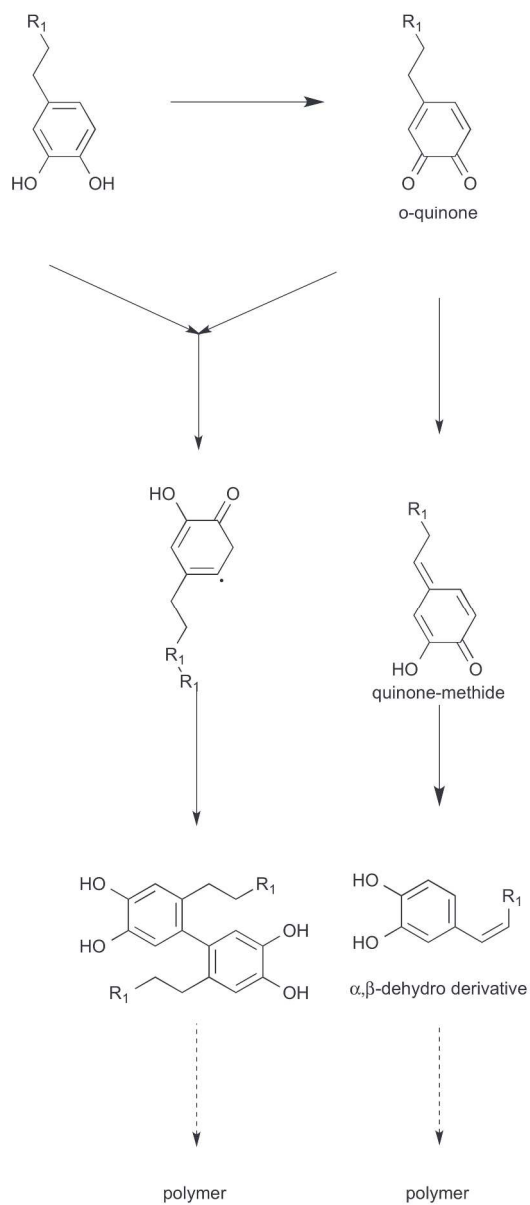


Figure 26. *o*-quinone forms crosslinks via two pathways: dismutation and tautomerization
166x381mm (600 x 600 DPI)

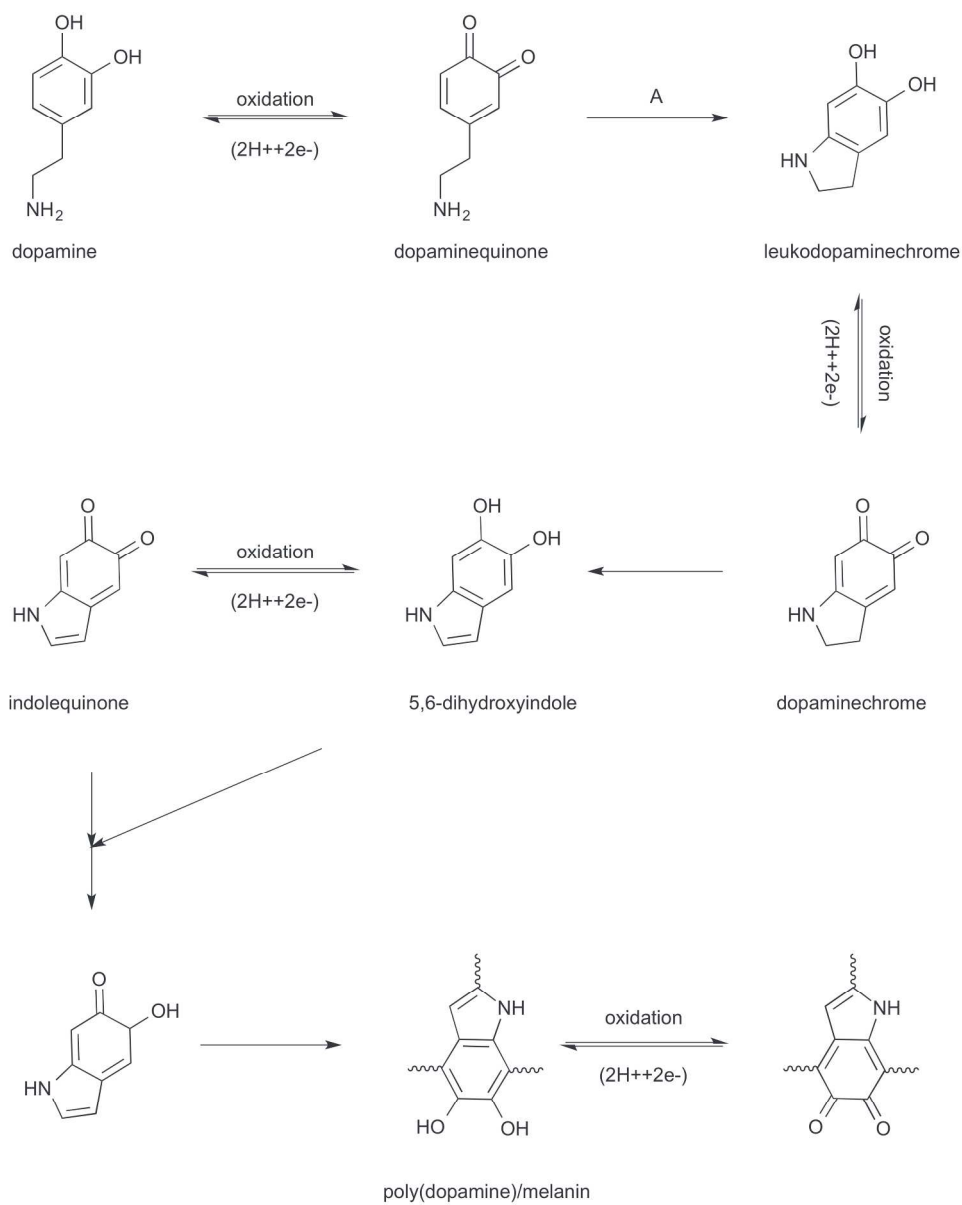


Figure 27. Reaction mechanism of melanin formation by dopamine oxidation.¹⁵⁵ Reproduced with permission from ref. 155. Copyright 2013, WILEY-VCH Verlag GmbH & Co. KGaA, Weinheim. 152x189mm (600 x 600 DPI)

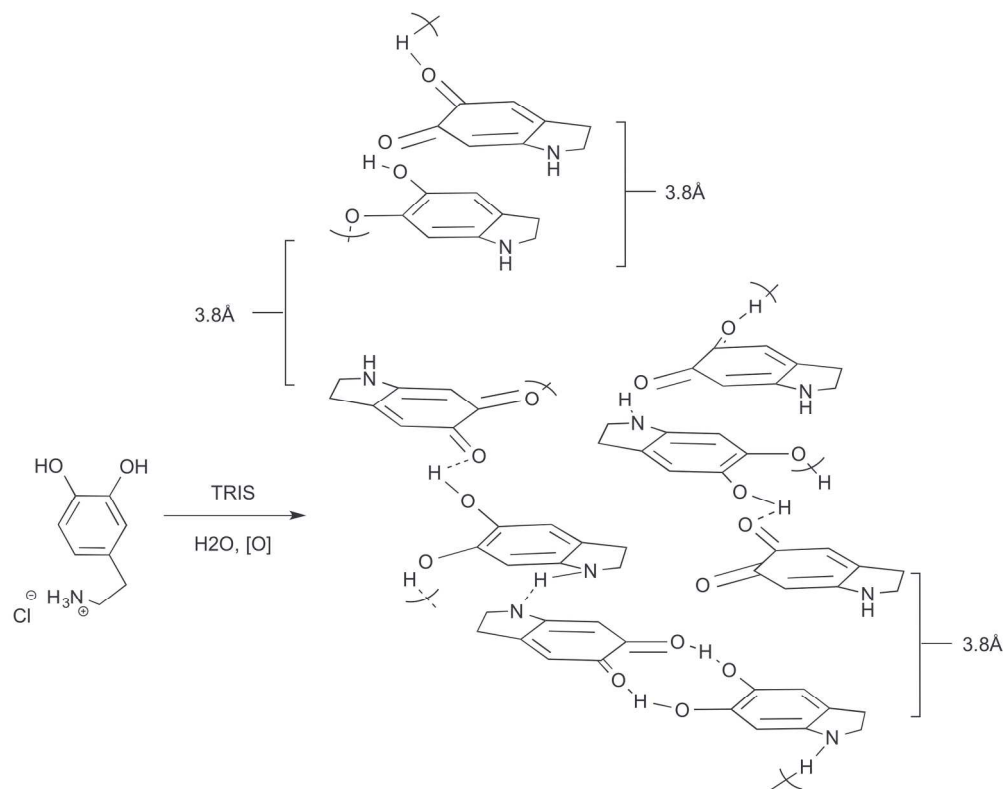


Figure 28. The PDA material is proposed to be comprised of intra- and interchain noncovalent interactions, including hydrogen bonding, π -stacking, and charge transfer.¹⁰⁰ Reprinted from ref. 100, Copyright 2010, with permission from Elsevier.
99x78mm (600 x 600 DPI)

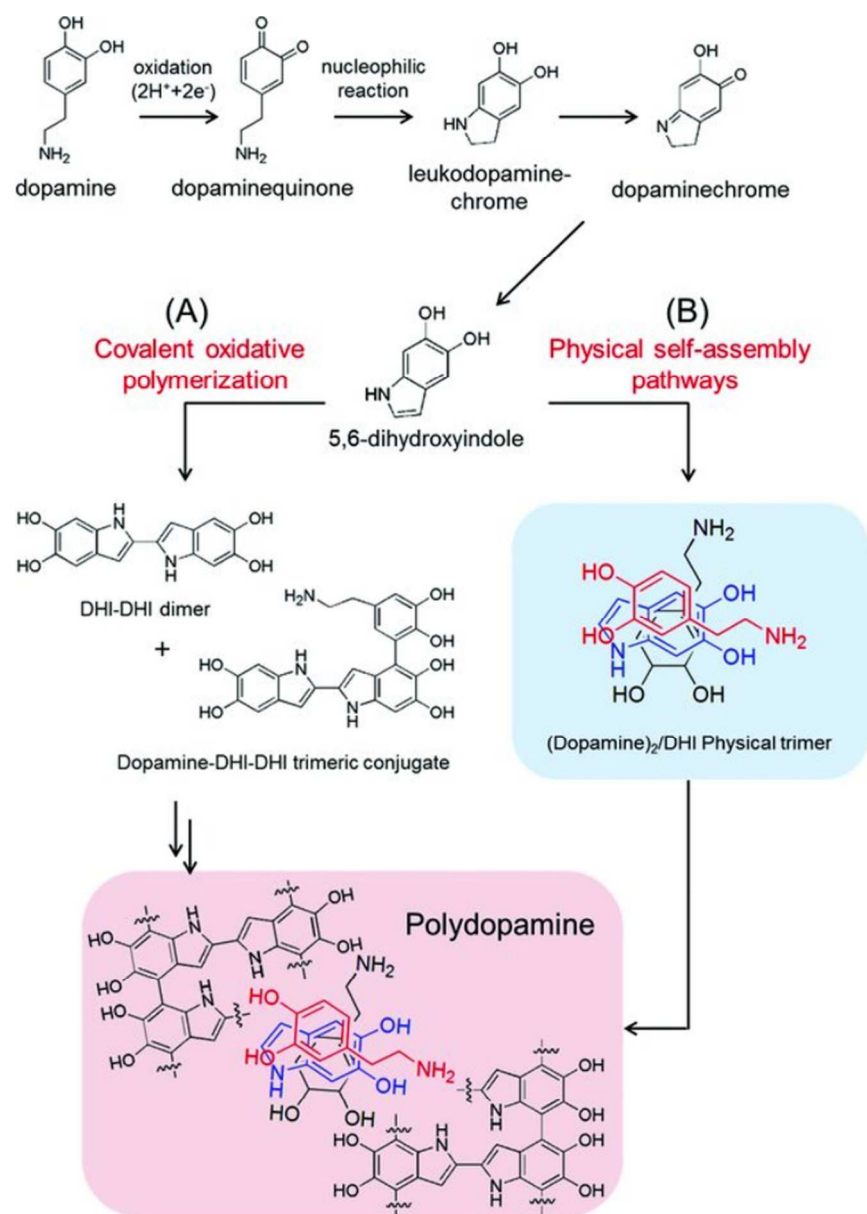


Figure 29. Polydopamine synthesis occurs via two pathways.¹⁰³ Reprinted with permission from ref. 103. Copyright (1982) American Chemical Society. 84x118mm (300 x 300 DPI)

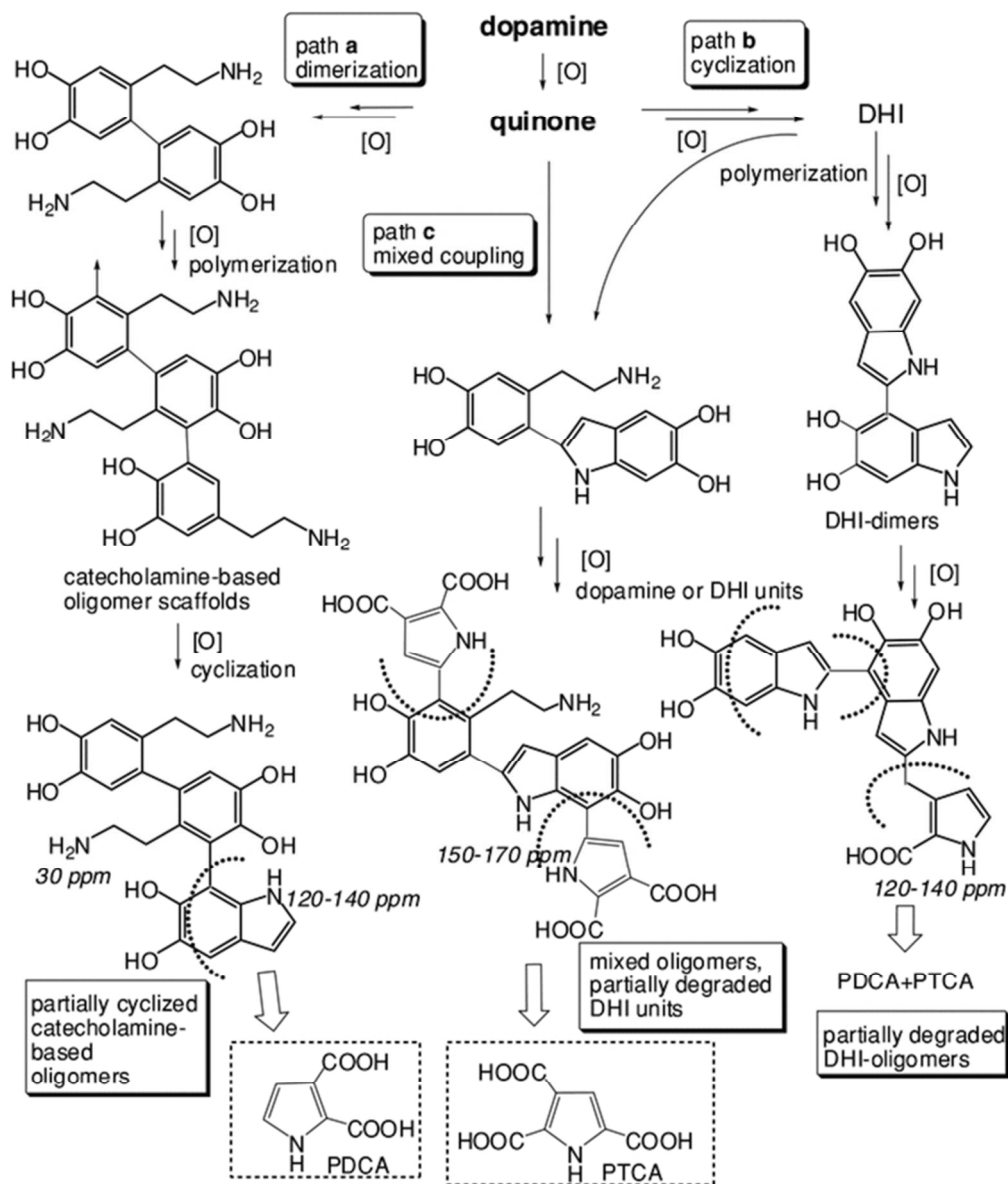


Figure 30. Simplified overall view of main reaction pathways involved in polydopamine formation.¹⁰⁴ Reproduced with permission from ref. 104. Copyright 2012, WILEY-VCH Verlag GmbH & Co. KGaA, Weinheim.

70x82mm (300 x 300 DPI)

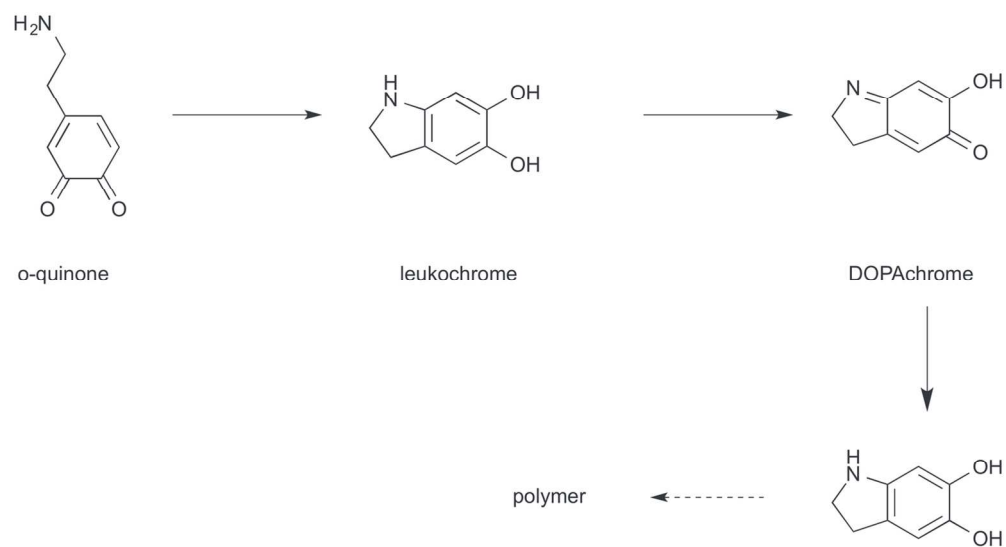


Figure 31. Polydopamine formation
65x35mm (600 x 600 DPI)

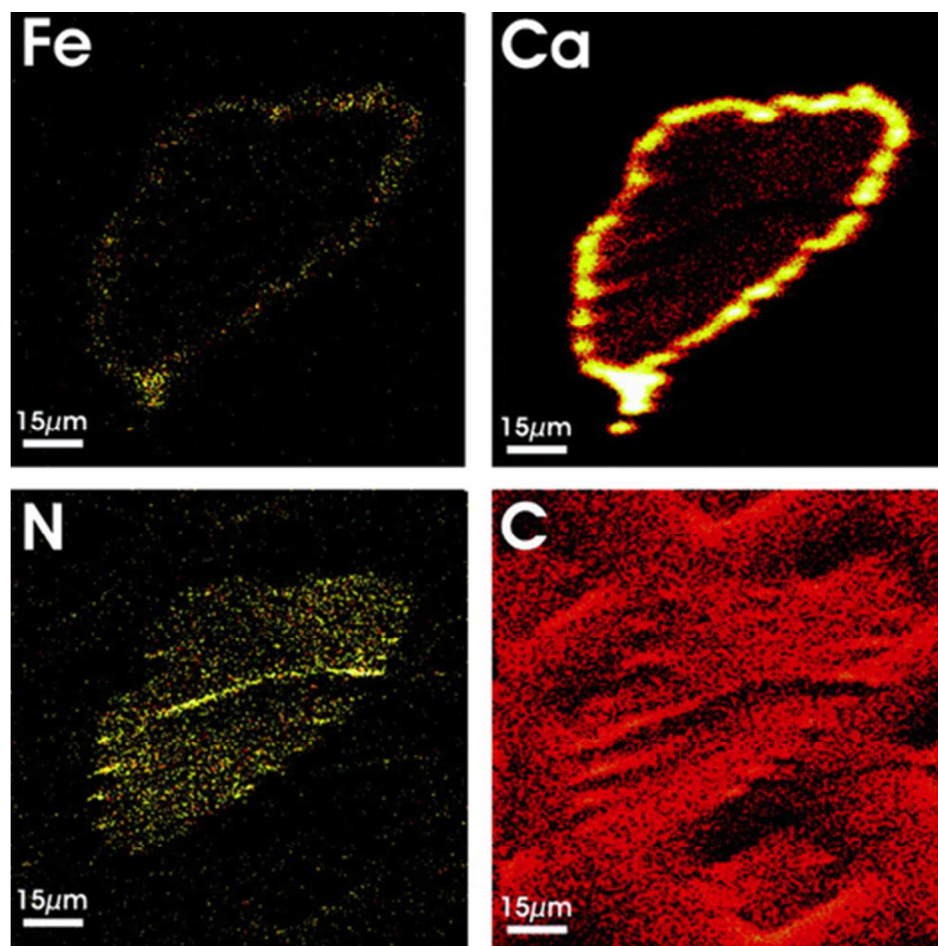


Figure 32. Maps of Fe, Ca, N, and C distributions in a transverse cross-section of a mussel thread generated using secondary ion mass spectroscopy (SIMS).¹¹⁶ Reprinted with permission from ref. 116. Copyright (2009) American Chemical Society
39x39mm (300 x 300 DPI)

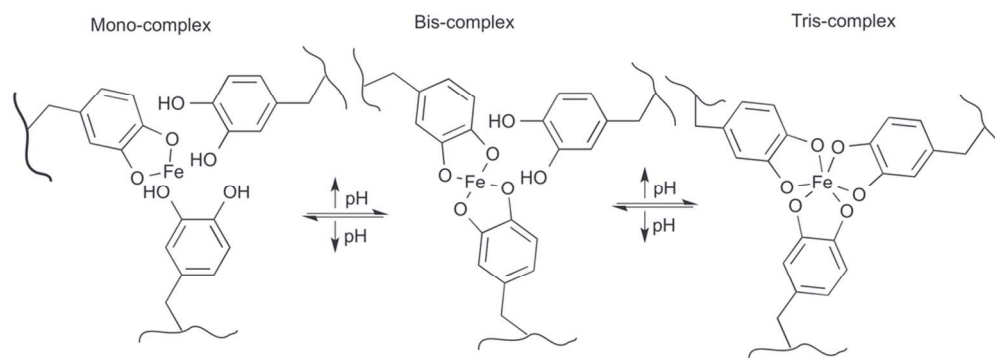


Figure 33: pH dependent stoichiometry of Fe^{3+} .¹³²
48x17mm (600 x 600 DPI)

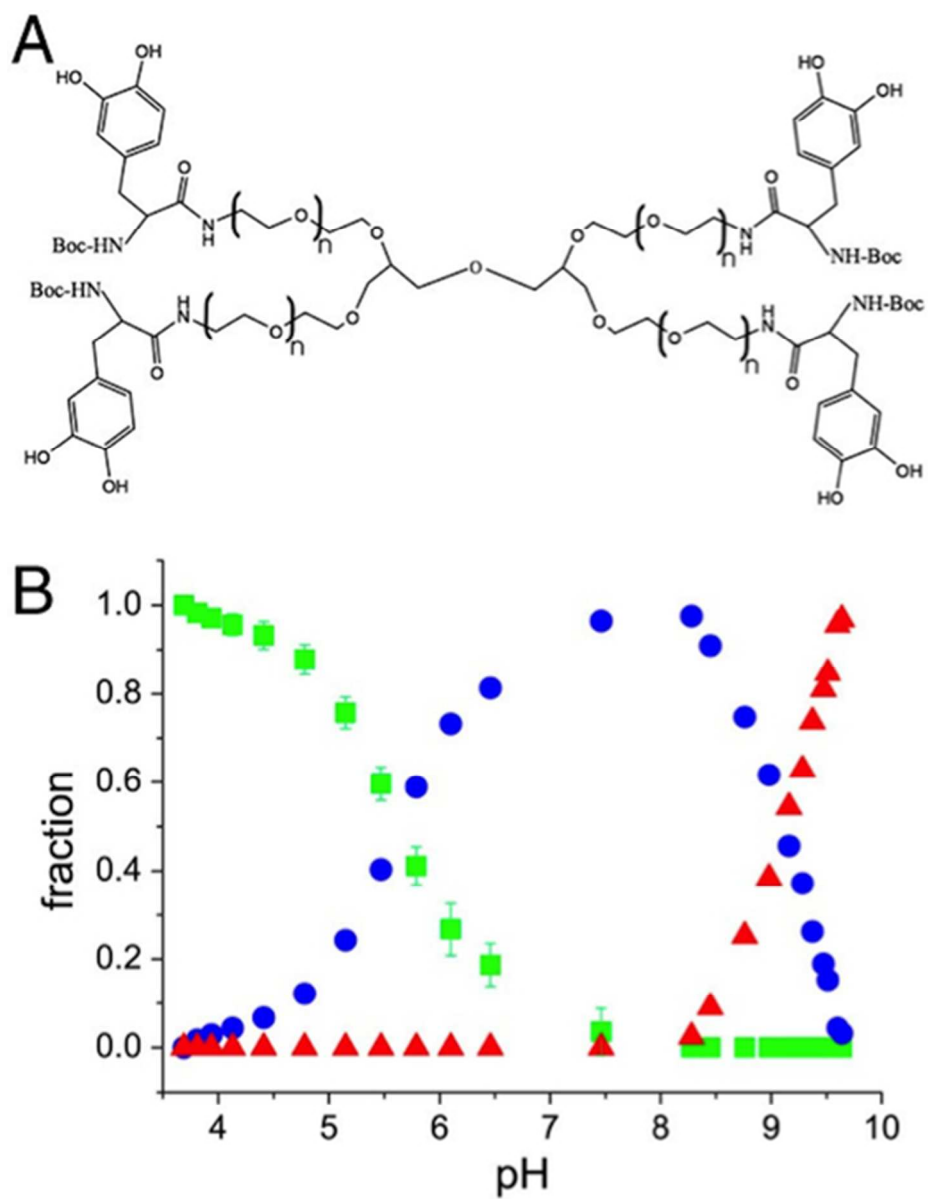


Figure 34. Catechol functionalized polyethylene glycol polymer. Relative fractions of mono bis and tris catechol-Fe³⁺ complexes in solutions with catechol-PEG with FeCl₃ (catechol: Fe molar ratio of 3:1) as a function of pH.¹³²
49x61mm (300 x 300 DPI)

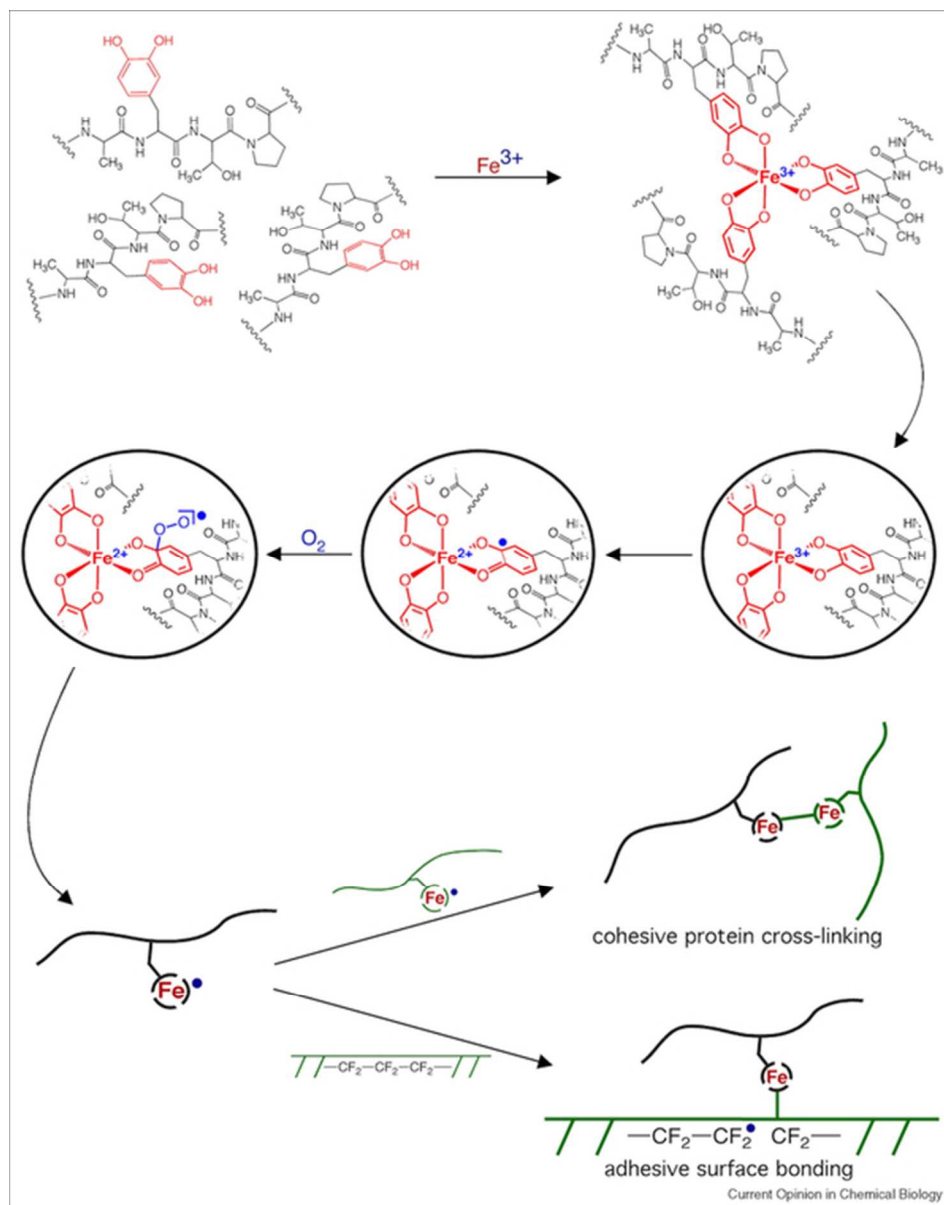


Figure 35. Proposed mechanism of iron mediated catechol crosslinking.¹⁴³ Reprinted from ref. 143, Copyright 2010, with permission from Elsevier.
50x64mm (300 x 300 DPI)

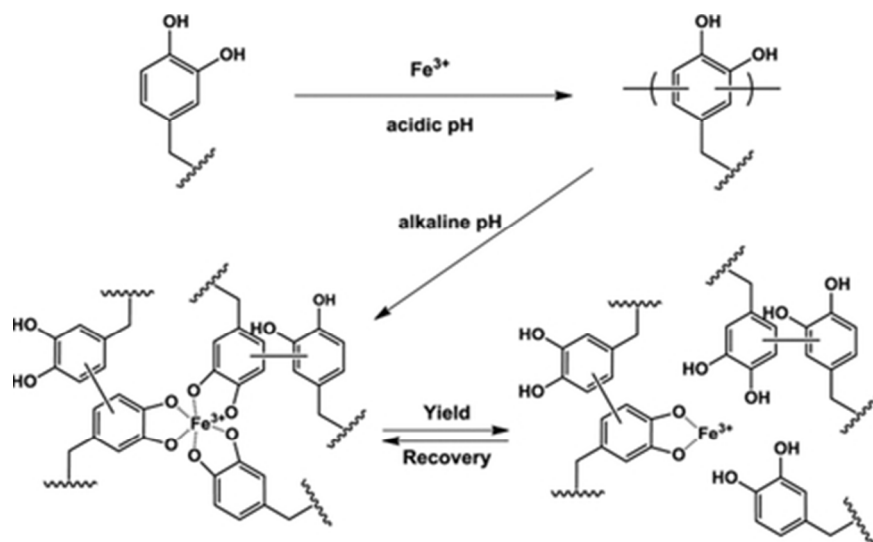


Figure 36. Proposed pH dependence of covalent and coordination bond formation mediated by Fe³⁺ in catechol functionalized polymers.¹⁴⁵ Reproduced with permission from ref. 145. Copyright 2013, WILEY-VCH Verlag GmbH & Co. KGaA, Weinheim.
36x22mm (300 x 300 DPI)

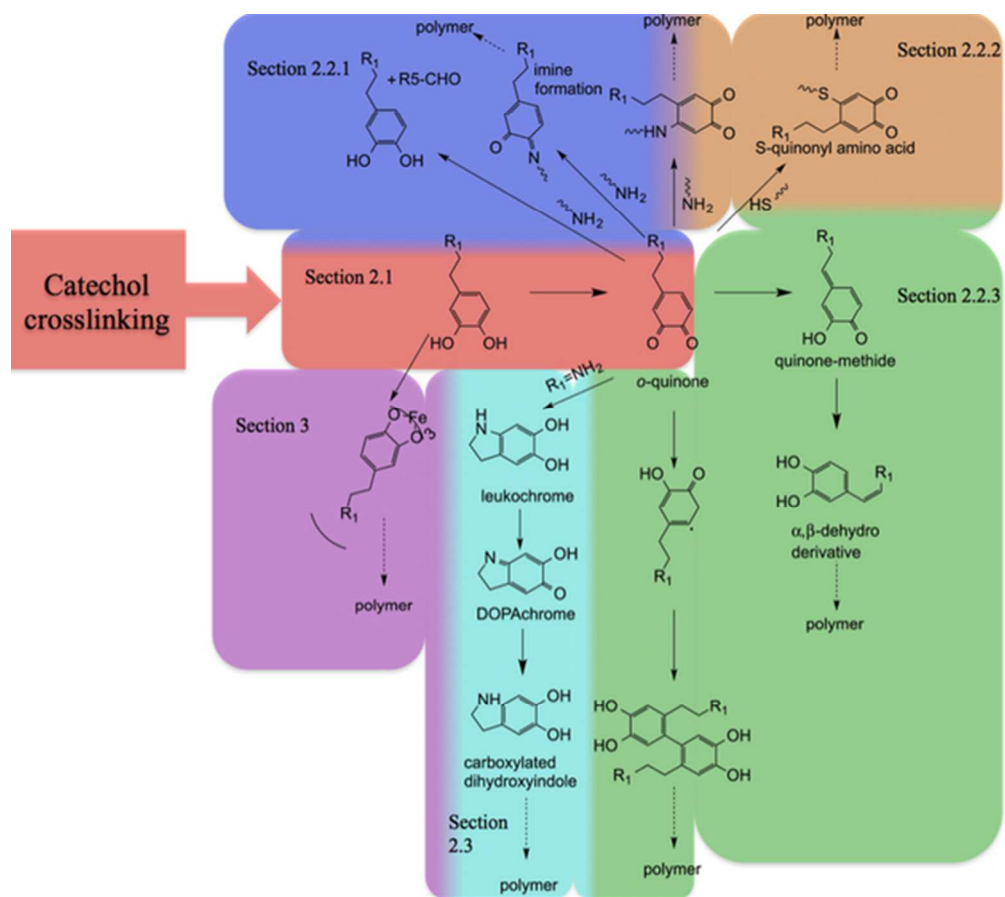


Figure 37. Crosslinking pathways of catechol-containing proteins
53x46mm (300 x 300 DPI)